Lawrence Berkeley Laboratory

UNIVERSITY OF CALIFORNIA

Charged-Particle Radiosurgery for Intracranial Vascular Malformations

J.I. Fabrikant, R.P. Levy, G.K. Steinberg, M.H. Phillips, K.A. Frankel, J.T. Lyman, M.P. Marks, and G.D. Silverberg

June 1991

Donner Laboratory

Biology & Medicine Division

DISCLAIMER

Charged-Particle Radiosurgery for Intracranial Vascular Malformations

J.I. Fabrikant, R.P. Levy, G.K. Steinberg, M.H. Phillips, K.A. Frankel,
J.T. Lyman, M.P. Marks, and G.D. Silverberg

Donner Pavilion and Donner Laboratory
Research Medicine and Radiation Biophysics Division
Lawrence Berkeley Laboratory
University of California
Berkeley, CA 94720

June 1991

CHARGED-PARTICLE RADIOSURGERY
FOR INTRACRANIAL VASCULAR MALFORMATIONS[1]

Jacob I. Fabrikant, M.D., Ph.D.,[*] Richard P. Levy, M.D.,[†] Gary K. Steinberg, M.D., Ph.D.,[‡] Mark H. Phillips, Ph.D.,[§] Kenneth A. Frankel, Ph.D.,[Φ] John T. Lyman, Ph.D.,[‖] Michael P. Marks, M.D.,[Ω] and Gerald D. Silverberg, M.D.[Θ]

[*] Professor of Radiology, University of California, San Francisco and Berkeley; Medical Scientist and Senior Scientist, Donner Pavilion and Donner Laboratory, Division of Research Medicine and Radiation Biophysics, Lawrence Berkeley Laboratory, University of California, Berkeley, California

[†] Assistant Adjunct Professor of Radiology, University of California, San Francisco; Medical Scientist and Staff Scientist, Donner Pavilion and Donner Laboratory, Division of Research Medicine and Radiation Biophysics, Lawrence Berkeley Laboratory, University of California, Berkeley, California

[‡] Assistant Professor of Neurosurgery, Stanford University School of Medicine, Stanford, California

[§] Assistant Adjunct Professor of Radiology, University of California, San Francisco; Staff Scientist, Donner Pavilion and Donner Laboratory, Division of Research Medicine and Radiation Biophysics, Lawrence Berkeley Laboratory, University of California, Berkeley, California

[Φ] Assistant Adjunct Professor of Radiology, University of California, San Francisco; Staff Scientist, Donner Pavilion and Donner Laboratory, Division of Research Medicine and Radiation Biophysics, Lawrence Berkeley Laboratory, University of California, Berkeley, California

[‖] Adjunct Professor of Radiation Oncology, University of California, San Francisco; Senior Scientist, Donner Pavilion and Donner Laboratory, Division of Research Medicine and Radiation Biophysics, Lawrence Berkeley Laboratory, University of California, Berkeley, California

[Ω] Assistant Professor of Radiology, Stanford University School of Medicine, Stanford, California

[Θ] Professor of Neurosurgery, Stanford University School of Medicine, Stanford, California

Direct correspondence to:

Jacob I. Fabrikant, M.D., Ph.D.
Donner Pavilion and Donner Laboratory
University of California at Berkeley
Berkeley, California 94720
Telephone: (415) 486-6118

SYNOPSIS

Under multi-institutional-approved protocols, nearly 400 patients with surgically inaccessible intracranial vascular malformations have been treated with stereotactic heavy charged-particle Bragg peak radiosurgery at the University of California at Berkeley, Lawrence Berkeley Laboratory. Doses ranged initially from 45 to 35 Gy equivalent (GyE), and currently, doses up to 25 GyE are being used for treatment volumes ranging from 0.1 cm³ to 70 cm³. Dose selection is dependent on size, shape, and location of the lesion and the volume of normal brain that must be traversed by the treatment beams. For complete radiation-induced obliteration, there is a relationship of dose and volume primarily, and location secondarily. When the entire arterial phase of an arteriovenous malformation (AVM) is included in the radiation field, the rates for complete obliteration 3 years after radiosurgery are: 90-95% for treatment volumes <4 cm³; 90-95% for volumes 4 cm³ to 14 cm³; 60-70% for volumes >14 cm³; and for all volumes (up to 70 cm³), approximately 80-85%. Serious complications approach 11% and include white matter changes and vasculopathy. Results on relationships between dose, volume, AVM obliteration, clinical grade, and complications following stereotactic heavy charged-particle radiosurgery are presented and discussed, with special emphasis on detailed clinical and radiologic follow-up in the University of California at Berkeley-Stanford University Medical Center collaborative clinical trial.

INTRODUCTION

At the University of California at Berkeley, Lawrence Berkeley Laboratory (UCB-LBL), heavy charged-particle beams are used for the stereotactic radiosurgical treatment of intracranial vascular disorders, mainly arteriovenous malformations (AVMs) [10,14,15,16,34, 35,67]. Beams of monoenergetic heavy charged particles are characterized by the deposition of a large fraction of their kinetic energy in a small volume at the end of their range — the Bragg ionization peak — and by the small angle of lateral scattering. The sharp lateral and distal edges of these beams and the increased dose in the Bragg peak furnish very precise means for localizing the radiation dose within the intracranial target lesion while sparing adjacent normal tissues [9,14,34,35,46,49]. At the same time, the optimal placement of such well-localized dose distributions requires very accurate imaging and precise computational treatment planning [14,15,34,35,44,46,50,60,62].

In 1954, the first stereotactic radiosurgical procedures using charged particles in humans were performed by Lawrence and Tobias and their colleagues at the UCB-LBL 184-inch synchrocyclotron [31,32,33,70,71,72]. Stereotactically directed focal pituitary irradiation with the "plateau" portion of the Bragg ionization curve was carried out with beams of protons and helium ions for pituitary hormone suppression in the treatment of patients with metastatic breast carcinoma. Subsequently, this method was applied to the treatment of proliferative diabetic retinopathy and pituitary adenomas. This experience with charged-particle radiosurgery in more than 800 patients, together with selected experimental animal studies and the physical properties of charged-particle beams, was reviewed recently in *Neurosurgery Clinics of North America* [35].

In 1980, we began using the Bragg peak of the helium-ion beam at the 184-inch synchrocyclotron for stereotactic radiosurgery of intracranial vascular disorders [15]. Thus far, we have evaluated and treated approximately 400 patients with surgically inaccessible intracranial vascular malformations, initially at the 184-inch synchrocyclotron (helium ions, 230 MeV/u) and currently at the Bevatron (helium ions, 165 MeV/u). The results of the treat-

ment have been evaluated radiographically using cerebral angiography, computerized tomography (CT), magnetic resonance imaging (MRI), and, in some series, positron-emission tomography (PET) and radioisotope scanning, as well as clinically with extensive neurologic examination [10,34,35,52,63,67]. The following report describes the method, treatment planning, clinical and neuroradiologic results, treatment complications and future directions and emphasizes recent clinical observations and conclusions drawn from the analysis of the UCB-Stanford University Medical Center (SUMC) collaborative clinical research program currently in progress [10,35,67].

METHODS

Patient Selection Criteria

Patients are evaluated for the radiosurgery protocol by a team of radiologists, radiotherapists, and physicists and the collaborative neurosurgical teams (including the referring neurosurgeon). Clinical protocols include collaborative programs with SUMC and the University of California Medical Center at San Francisco (UCSF). Patients are considered to be candidates for the clinical-trial protocol if they have been symptomatic and have a history or clinical evidence of previous hemorrhage, seizures, disabling headaches, or fixed or progressive neurologic dysfunction. Some patients are referred to the protocol after having undergone subtotal surgical resection or clipping of accessible feeder vessels or interventional neuroradiologic procedures (e.g., flow-directed or intraoperative embolization).

Patients with AVMs considered to be surgically accessible by our multi-institutional protocol team are offered operative resection as primary treatment. Embolization may be recommended in preparation for radiosurgery of an AVM in cases where a limited number of identifiable and accessible feeding vessels exist. Here, the aim is to reduce the rate of blood flow through the AVM and the overall volume of the AVM, allowing for a decrease in size of the target volume to be treated, if at all possible. Following the multidisciplinary evaluation, each patient accepted in the protocol is categorized into one of four

treatment groups: stereotactic heavy charged-particle radiosurgery, embolization followed by stereotactic radiosurgery, subtotal surgical resection or clipping of feeding vessels followed by stereotactic radiosurgery, or subtotal surgical resection and embolization followed by stereotactic radiosurgery. Patients with angiographically occult vascular malformations (AOVMs) are accepted into the radiosurgery program only if there is clinical and radiologic evidence of hemorrhage and the AOVM is considered surgically inaccessible or the patient is unwilling to undergo surgery. No asymptomatic patients are accepted into the protocol.

Clinical Evaluation

Clinical follow-up to evaluate health outcomes in all patients is defined in protocols provided to all referring physicians. Follow-up information is obtained frequently, at least every 6 months. Patients are examined to assess neurologic status and change in clinical grade, evidence of hemorrhage, and complications or sequelae. The frequency and severity of headaches and seizures, and neurologic dysfunction in patients who presented with progressive nonhemorrhagic neurologic dysfunction, are described as *improved, unchanged,* or *worse.* In the clinical grading before and after radiosurgery, we have chosen to use the scale of Drake [7,8]; each patient's neurologic status is described as *excellent* (able to work with no neurologic handicaps), *good* (having a neurologic deficit but able to work and live independently), *poor* (having a severe, disabling neurologic deficit and dependent on nursing or family help), or *dead.*

We are very conservative in scoring complications of the radiosurgical procedure. All changes observed on MRI and CT images and cerebral angiograms that appear to be a direct or indirect response to radiation-induced injury, other than obliteration of the abnormal vascular shunts of the AVM, and any treatment-related neurologic dysfunction, are considered to be sequelae of the treatment procedure [10,34,36,52,63,67]. Clinical complications are categorized as *major* (new neurologic deficits that result in a worsening in the patient's functional grade) or *minor* (neurologic deficits that are clinically evident but do

not change the functional grade). Because focal irradiation does not induce immediate endovascular thrombosis of the malformation, but gradual obliteration over the course of 1 to 3 years, during which time the patient remains at risk for intracranial hemorrhage, we consider post-treatment hemorrhage separately from radiation-associated complications or sequelae.

Neuroradiologic Evaluation

Stereotactic neuroradiologic evaluation prior to radiosurgery includes cerebral angiography, CT scans, and MRI scans. The composite information from these studies is used to determine the radiosurgical target and treatment volume (see *Stereotactic Localization*, below). AVMs are measured according to both *treatment volume* and *angiographic volume*. The *treatment-volume* method much more closely approximates the true volume of the lesion, but the *angiographic-volume* method is more readily amenable to serial quantitative volume analysis and reasonably describes proportional response [61].

Treatment-volume determination has been described previously [60]. Briefly, the noncontrast stereotactic CT images are loaded into a VAX 11/780 computer, and the coordinates of the ends of two of the wire reference markers (row, column, and CT slice number) on the stereotactic frame are obtained (see below). This information, along with the slice thickness (3 mm) and pixel size (0.78 mm), is used to map each point of the angiographically determined digitized target contours onto the CT-image data set. At each level of the angiographic image (along the cranial-caudal axis) that corresponds to a CT slice, the dimensions of the anteroposterior and lateral projections of the AVM are used as the major and minor axes of an ellipse. Thus, the AVM target volume in the CT image set is a series of ellipses of thickness equal to the slice separation, stacked one on top of the other. Pronounced deviations from the true shape of the lesion by such elliptical contours are occasionally evident from CT or MR images, such as when the AVM extends around a ventricle or closely follows the edge of some readily imaged brain structure (e.g., corpus callosum). In these cases, the

CT target contours are redrawn on the CT images to conform to the actual target geometry. *Angiographic volume* is derived from a rectangular parallelopiped circumscribing the angiographically determined maximum projected length, width, and height of the arterial phase of the AVM [51].

The incidence of cerebral arterial aneurysms among patients with untreated AVMs has been variously estimated as being between 3% and 9% [42]. Therefore, the angiograms of all patients are examined for associated aneurysms. Aneurysms in vessels feeding the AVM or associated with the circle of Willis are treated surgically before (or immediately after) radiosurgery of the AVM. Intranidal aneurysms (i.e., those seen early in the arterial phase of the angiogram and within the AVM core) appear to be associated with an increased risk of AVM hemorrhage and therefore are considered separately from arterial aneurysms [53].

Following stereotactic radiosurgery for angiographically demonstrable AVMs, cerebral angiograms are obtained every 12 months or until complete vascular obliteration has occurred. Angiographically defined responses are classified as *complete obliteration* (the absence of any demonstrable arteriovenous shunt), *partial obliteration* (a 10-99% reduction in volume but with persistent arteriovenous shunting), or *no change* (less than 10% reduction in volume). All measurements of angiographic volumes, initially and after treatment, are performed by the same neuroradiologists. Mann-Whitney tests [59], Kaplan-Meier plots [21], and Cox tests [5] are used for statistical analysis of rates of angiographically detectable obliteration among patient groups with different treatment doses and AVM volumes [67].

Unless contraindicated, MRI is carried out at 6-month intervals, and CT at 12-month intervals, for the first 4 years following radiosurgery to assess the vascular response, to identify early or delayed radiation injury and/or edema in the brain, and to guide appropriate management. Patients with AOVMs are followed up with MRI every 6 months and CT scanning yearly; follow-up angiography is not performed in these patients. Some patients are evaluated with serial PET scanning to characterize pathophysiologic changes in regional cerebral blood flow (rCBF), glucose metabolism, and blood-brain-barrier (BBB) integrity

after radiosurgery. These changes are correlated with those seen in sequential MRI [73].

Charged-Particle Beams

The use of multiple convergent charged-particle beams with the appropriate depth of penetration enables a high dose of radiation to be delivered to a well-defined region with no or minimal radiation effect in the surrounding tissues. This technique uses the favorable physical properties of the heavy charged-particle beams, which include the Bragg peak, the minimal multiple scattering and range straggling, and sharp beam profiles (Fig. 1) [35,47,48,49]. The maximum range of the 230 MeV/u helium-ion beam at the 184-inch synchrocyclotron is 316 mm in water; this is much greater than is required for the Bragg-peak irradiation of intracranial targets. Because the synchrocyclotron is a fixed-energy machine, a large fixed absorber is placed in the beam line to decrease the maximum available range [35]. The range of the beam in configuration for stereotactic radiosurgery is 145 mm. Additional absorbers then are added to obtain the required residual ranges for each treatment port. Typically, the thickness of the target volume in the direction of the beam path is greater than the width of the Bragg peak. Therefore, to achieve the desired dose distribution and dose uniformity, the beam must be modulated with a rotating acrylic propeller so that the particles stop over a greater volume (Fig. 2) [35].

The range-modifying material and the collimation in the beam line affect the lateral or transverse beam profiles. A sharp profile is desirable to minimize the dose to the normal tissues immediately adjacent to the target volume; this is critical in the brain and spinal cord. The measured penumbra (distance between the 90% and 10% dose profiles) increases with the residual range of the beam. The sharpest transverse profiles are obtained when the final collimator is at the surface of the patient and when the shortest residual range is used (Table 1) [41,46,48,49].

[TABLE 1 ABOUT HERE]

The LBL Bevatron accelerator was first used for radiosurgical treatment in 1988. The

maximum range of the 165-MeV/u helium-ion beam is 180 mm in water. Dynamic beam stacking was implemented at the Bevatron, replacing rotating lucite propellers as a means of spreading the heavy charged-particle Bragg peak to the desired width, matching the region and configuration of high dose to the dimensions of the target volume [41,60]. Comparison of the helium-ion beams from the two accelerators (Table 1) illustrates the improvement in the beam characteristics if the appropriate beam energy is available [46,47,49]. Some of the differences between these two beams may be due to the energy spread of the extracted beam, since the beams are from different accelerators. However, the maximum ranges of the two helium beams differ by a factor of about two. The lower beam-extraction energy available at the Bevatron results in less range straggling (i.e., a sharper Bragg peak) and less scattered radiation [46].

Charged-particle beams heavier than protons have an additional biologic advantage for radiosurgery of intracranial lesions. The Bragg ionization peak has a greater relative biologic effectiveness (RBE) per unit physical dose than do x-rays, gamma rays, or protons. Based on extensive experimental evidence, we have concluded that, for the helium-ion beams at the Bevatron, in the dose range used for stereotactic radiosurgery in the brain, the RBE of the plateau region relative to 250-kVp x-rays is approximately 1.0. The RBE varies as the Bragg peak is spread out, but averages approximately 1.3 in the peak, that is, the biologic effectiveness is 30% greater than for the same physical dose in the plateau portion of the beam or for photons [3,44]. Accordingly, for comparison with conventional radiotherapeutic and radiosurgical dose levels, the physical dose of the charged-particle irradiation is multiplied by the value of the RBE to obtain the equivalent dose level used. For example, a physical dose of 19.2 Gy of helium-ion Bragg peak irradiation is the biologic equivalent of 25 Gy of 250-kVp x-rays and is referred to as 25 Gy equivalent (25 GyE).

Stereotactic Localization

The application of heavy charged-particle Bragg peak radiosurgery for the treatment of intracranial vascular and other disorders requires a system of precise patient head immobi-

lization and stereotactic localization of defined intracranial targets. Such a system must be adaptable and reusable to enable stereotactic neuroradiologic procedures to be used for target definition and localization, complex treatment planning, radiosurgical treatment, and selected follow-up neurodiagnostic studies. We have developed a removable stereotactic frame-mask system that incorporates an individualized thermoplastic immobilizing head mask and stereotactic frame. This device permits accurate and reproducible positioning of the patient's head for the different neuroradiologic procedures, including single-fraction or multifraction radiosurgical treatment at the 184-inch synchrocyclotron and the Bevatron. The stereotactic frame-mask system consists of four parts (Figs. 3 and 4): a plastic mask prepared for each patient to immobilize the patient's head, a lucite-graphite mounting frame, a set of fiducial markers, and interfaces between the frame for immobilization and fixation to various diagnostic and therapeutic radiologic couches [50]. The relationship between each component provides a system that, in more than 1200 patients, has proven to be safe, reliable, and noninvasive and does not require rigid bone fixation [35,50].

Stereotactic information obtained from the angiograms, CT, and MRI must be correlated to obtain the exact size, shape, and position of the intracranial lesion (Fig. 5). Ultimately, it is necessary to position the AVM at the isocenter of the specially constructed radiosurgery patient positioner, the Irradiation Stereotactic Apparatus for Humans (ISAH) (Figs. 2 and 6) [45]. For this purpose, the stereotactic information obtained from the neuroradiologic studies is correlated with localization radiographs obtained in the treatment facility at the heavy-ion accelerator at the time of radiosurgery. ISAH has been shown to have an accuracy and precision that is 0.1 mm in translation and 0.1 degree in rotation [45].

The target for radiosurgical irradiation is determined from selected orthogonal angiograms. From these films, geometric factors, coordinates of the intracranial target, and exact dimensions of the target are obtained. Correlation of the angiographic and CT image markers enables the transfer of the target volume and location to the CT images [60]. Similarly, correlation between MRI and CT image markers allows transfer of information

between the two [62]. After transferring the AVM-target contours to the three-dimensional CT data, we calculate the treatment planning parameters, and obtain the coordinates of ISAH necessary to position the center of the lesion at the isocenter of ISAH. The CT data provide the information needed to construct a set of beam ports that will yield the desired dose distribution at the site of the vascular lesion.

The digitized angiographic images are used to calculate the initial position of the patient-positioning couch and provide the basis of computer-generated overlays of the frame, target, and midplane bony landmarks of the skull on localization radiographs [60]. The radiosurgical procedure requires that the target be localized precisely at the intersection of the charged-particle beam and the isocenter of ISAH [45]. When the stereotactic frame is mounted on ISAH, a known set of coordinates positions the center of the frame at the isocenter ("frame zero"). A computer program calculates the offset of the target from frame center and, using the ISAH coordinate set for frame zero, calculates the coordinates that will place the center of the target at isocenter for beam delivery [60].

Final alignment of the patient's head (and AVM target) is assured by comparing lateral and anteroposterior radiographs taken on ISAH to the computer-generated digitized overlays of the frame, skull, and angiographically determined target [60]; the overlays can be correlated with MRI as needed (e.g., for AOVMs). Figure 7 illustrates the lateral and anteroposterior views of a computer-generated overlay, with stereotactic frame fiducial markers, treatment target, and midplane landmarks clearly identified. The isocenter is located at the intersection of the stereotactic-frame fiducial markers in the "zero-position" view (top) and at the center of the target in the "treatment" view (bottom). The different geometries of these two positions are clearly demonstrated by viewing the fiducial markers. The changes in the relative positions of the midplane landmarks and target contours are less readily apparent, but are also present in the image.

With the stereotactic-localization system and the radiosurgical treatment planning procedures developed at UCB-LBL, we are able to reposition the patient's head in the mask to

a precision of approximately 1 mm or less in each of three orthogonal directions in repeated diagnostic and therapeutic sessions and to contour the intracranial target reliably to this accuracy [50,60,62]. Misalignments in either translation or rotation then are corrected to within 0.5 mm with the use of localizing radiographs. The achievement of this accuracy is determined by the goodness of fit between the localizing radiographs and the computer-generated overlay of the stereotactic angiographic films (Fig. 7). The positioning errors are attributed almost entirely to the repositioning of the patient within the mask.

Treatment Planning and Dose Distributions

The optimal treatment-planning procedure for heavy charged-particle Bragg peak radiosurgery presents a number of problems not encountered in conventional radiotherapy treatment planning [74]. The procedure consists of a series of stages involving sequential neuroradiologic imaging studies, computer-assisted correlations among the different types of radiologic imaging information, calculations of the dose distributions, and application of the output of these steps to the radiosurgical procedure [60,62]. The neuroradiologic data are used for target-volume contouring and for calculation of relative stopping-power values for charged particles. Multiple entry angles, beam ports, and tissue compensation are chosen to confine the high-dose Bragg ionization peak to the AVM, while protecting adjacent critical structures of the brain, such as the brain stem, central nuclei, and optic chiasm (Fig. 8) [10,14,15,34,35]. Several prospective treatment plans (isodose contour displays) are calculated individually for each patient. The best plan finally is chosen from a number of potentially satisfactory plans.

The size, shape, and location of an AVM are determined most precisely by stereotactic angiography. However, angiography does not determine the relationships of the AVM to surrounding brain structures, nor does it provide information to calculate the range of charged-particle beams. CT can be used for range calculations and to demonstrate relationships to adjacent anatomic structures but does not delineate the AVM precisely. Contrast-enhanced CT often highlights the AVM, but feeding and draining vessels and the

AVM core containing the abnormal vascular shunts are not well differentiated from one another. To utilize fully the unique physical characteristics of the charged-particle beams for safe and effective treatment, the vascular target volume must be defined and located precisely within a reproducible three-dimensional reference frame, the physical properties of the materials to be traversed by the beam must be determined accurately, and the patient must be positioned exactly with respect to the beam [60,62].

The stereotactic frame and head-immobilization system are used to correlate the multi-vessel angiograpic and CT images [50,60]. The contours of the AVM target derived from the angiograms and transferred to the noncontrast CT images form the basis for the stereotactic treatment-planning procedure. The CT data provide detailed information regarding the physical characteristics of the tissues on a pixel-by-pixel basis as well as information about the correlative neuroanatomy of the head and brain. A computer program is used to transfer the target outline from the angiographic films to the CT data to calculate the charged-particle treatment parameters, that is, the treatment plans. Via geometric optics, the digitization program uses the position of the fiducial markers of the stereotactic frame as they appear on the radiographs in conjunction with their known position on the frame to calculate the relevant radiologic imaging parameters (Fig. 7) [60]. The CT data and the digitized target contours derived from each axial slice are reformatted to provide views through the lesion in three dimensions, and relevant views through the lesion are obtained in the axial, coronal, and sagittal planes [60].

The CT data and target contours are used to calculate the residual range and compensation for each treatment beam port [46,47,60]. The helium-ion beam is extracted from the accelerator at a fixed energy (at the 184-inch synchrocyclotron, 230 MeV/u for a water-equivalent range of 32 cm; at the Bevatron, 165 MeV/u for a water-equivalent range of 18 cm) [46,49]. The water-equivalent path length through the head is calculated for each beam port, and the amount of absorber necessary to place the distal edge of the spread-out Bragg peak at the distal edge of the lesion is obtained. Inhomogeneities in the tissues to be

traversed or irregularities in the shape of the lesion are accounted for by the use of tissue-equivalent compensators positioned in the beam path, which adjust the placement of the distal portion of the peak to the lesion boundaries across the profile of the beam [35,60,74].

The number of treatment ports used varies from one to seven, most commonly four, and is based on the requirement to treat the lesion with an optimal dose distribution and to minimize risk to the adjacent normal tissues [49]. The properties of the beams, the size of the lesion, the location of the volume to receive the highest dose, and the total dose are factors that affect the number of ports, entry angles, and dose-configuration patterns chosen. Most frequently, four noncoplanar beams are used, angled to avoid overlapping high-dose "hot-spots." Acceptable treatment plans for all patients are obtained without requiring a beam range greater than 150 mm in water.

The width of the spread-out Bragg peak for each beam port is calculated to provide maximal coverage of the lesion on all slices. Smaller targets usually require 5- to 10-mm modulation of the helium-ion beams; larger lesions typically do not need more than 25- to 35-mm modulation [35]. The beams generally are collimated with either a circular or an elliptical brass aperture when small lesions are treated. With larger or irregularly shaped vascular malformations, individually designed apertures are fabricated to match the beam shape with the orthogonal angiographic projections of the AVM [35,60]. Circular or elliptical brass apertures are modified to the desired shape and size with cerrobend (a low-melting temperature dense alloy) [35]. The maximum dimension of the apertures is usually less than 40 mm but can exceed 60 mm as required. Radiosurgery is performed based on the final treatment plan generated, assuring a relatively homogeneous dose distribution with the 90% isodose surface contoured to the edge of the lesion to the extent possible [10,14,15,34,35].

The dose to critical normal structures adjacent to the AVM is considerably less than the dose to the target volume, because at the 184-inch synchrocyclotron, the fall-off to 10% of the central axis dose occurs within 4-6 mm distally and is within 2-3 mm along the lateral margins of the helium-ion beam. At the Bevatron, the distal dose fall-off is

considerably less, within 2-3 mm. To the extent possible, the radiation beams and entry angles are planned to confine the radiation solely to the ipsilateral hemisphere. Figures 8 and 9 are examples of the isodose contour displays of treatment plans for radiosurgery at the 184-inch synchrocyclotron in two patients with AVMs, one with a small volume and another, a large volume (see also Fig. 10). In both cases, the beams were stopped without crossing into the contralateral hemisphere. It is particularly for the treatment of moderate-sized to large AVMs that heavy charged-particle Bragg peak radiosurgery demonstrates the considerable advantages offered by the physical and biologic characteristics of the heavy-ion beams [10,13,34,35,61].

The radiosurgical treatment plan is designed to ensure irradiation of the main arterial feeders and the core of abnormal shunting vessels of the AVM proper and to include, as completely as possible, the whole cluster of pathologic shunting vasculature within a relatively homogeneous radiation field. The entire compartment of this vascular unit is considered the AVM core and must be included in the target volume. Partial-volume radiosurgery has proven to be unsatisfactory, resulting in residual vascular shunts that remain prone to intracranial hemorrhage [36].

A special situation arises in treatment planning for radiosurgery of AOVMs [37]. We have developed methods for correlating stereotactic MRI and CT images to determine the location, size, and shape of the target volume [37,62]. The procedure enables the transfer of CT-calculated isodose contours to the MR images to aid in the determination of optimal treatment plans. In the patient whose treatment planning is illustrated in Figure 11, there was evidence of intracranial hemorrhage on CT images: cerebral angiography revealed no abnormal vasculature. The AOVM in the brain stem is visible on the MR images as a region of high-intensity signal surrounded by regions of low-intensity signal. Image correlation techniques are used to transfer the contours of the lesion as drawn on MR images to the corresponding CT images [22]. Fiducial markers are placed on the mask in such a way that at least four, but most often six to ten markers, are visible on axial, coronal, and

sagittal images. The coordinates of each fiducial marker are recorded on both the MRI and CT images, and a least-squares fit is calculated that maps any set of points from MRI to CT (and vice versa). This fit corrects for translational and rotational errors as well as for linear "stretching." A three-dimensional treatment plan is calculated on the axial and sagittal CT slices through the lesion. Isodose contours display the dose distributions relative to the lesion and critical adjacent neural structures on corresponding axial, coronal, and sagittal MR images. The dose to anatomic structures that are imaged with MRI are readily identified (Figs. 11 and 12), and this information aids in decisions regarding a particular treatment plan (e.g., beam angles and directions, aperture shapes, and compensation).

Radiosurgical Procedure and Treatment Dose

Once the target center is located at the isocenter of the stereotactic-localization system (ISAH), the beam is delivered through a number of ports by rotating the patient's head to a predetermined fixed position [10,14,15,34,35]. The radiosurgical procedure typically requires about 30-60 minutes; each beam port requires 10-15 minutes for patient positioning and 1-3 minutes for beam exposure. A simulation procedure of the actual treatment is carried out beforehand to assure the accuracy of treatment planning and patient familiarity with the equipment and procedure and to anticipate any untoward patient problems. This simulation tends to shorten the time necessary for patient positioning during the treatment. All patients are treated on an outpatient basis. Patients begin receiving a course of low-dose oral dexamethasone the day before treatment; this is tapered off over the next 2 weeks.

Initially, during the early stages of the clinical trials, treatments usually were given in up to three or four fractions, larger treatment volumes receiving the greater number of fractions. We decreased the number of fractions as our clinical experience grew and now generally use only one or two fractions, depending on the size of the target volume and the volume of normal brain tissue that the beams must traverse.

Currently, total doses of 15-25 GyE are delivered to treatment volumes ranging from 0.1 cm^3 to 70 cm^3. Initially, the dose-searching protocol for the first 100 patients included a

range of 35-45 GyE. Because AVM obliteration occurred at the lower end of this dose range, the protocol examined incrementally lower therapeutic doses to attempt to decrease the risk of complications [10,13,34,35,36,63,67]. The dose for each patient is selected individually and depends on the size, shape, and location of the AVM and several other factors, including the volume of normal brain tissue that must be traversed by the plateau portion of the charged-particle beams [10,34,35,67].

RESULTS

Patient Selection

Of the nearly 400 patients with intracranial vascular malformations who have been evaluated and treated using stereotactic heavy charged-particle (helium-ion) Bragg peak radiosurgery at the UCB-LBL 184-inch synchrocyclotron and Bevatron [10,11,13,14,15,34, 35,67], 50 patients were aged 6 to 18 years [34], and 42 patients had AOVMs [36]. Fifty-two percent were female and 48% were male; 17% were 6-20 years old, 61% were 21-40 years old, 18% were 41-60 years old, and 4% were over 60 years old at the time of treatment. About 50% of the patients had no interventional therapy prior to radiosurgery, but many had undergone some form of AVM surgery (29%) and/or interventional neuroradiologic procedure such as embolization (21%). Various combinations of therapeutic procedures were carried out in certain patients to decrease the volume and/or blood flow of the AVM in preparation for radiosurgery. Some patients had one or more additional procedures (e.g., arterial aneurysm repair) not intended to decrease malformation size or rate of blood flow. Using *treatment-volume* criteria (described earlier) [60], 44% of AVMs measured between 0.1 cm^3 and 4 cm^3, 36% between 4 cm^3 and 14 cm^3, and 20% greater than 14 cm^3; the largest AVM treated was 70 cm^3.

Our UCB-SUMC collaborative program recently reported the clinical results of a cohort of 86 consecutive patients with angiographically demonstrable AVMs [67]. There were 47 females and 39 males, ranging in age at the time of treatment from 9 to 69 years (mean, 33 years). Many patients presented with more than one symptom; 60 had hemorrhaged, 11 had neurologic deficits unassociated with hemorrhage, 35 had seizures, and 40 had headaches. Sixty patients (70%) were graded clinically as *excellent* before radiosurgery, 24 (28%) as *good*, and 2 (2%) as *poor*. Prior to radiosurgery, 17 patients had undergone partial resection of their AVMs, 7 had flow-directed embolization, and 5 had both embolization and surgery. Nearly half of these patients (44%) had AVMs located in the brain stem, corpus callosum, thalamus or basal ganglia, and most of the remainder had large malformations in critical areas of the cerebrum—the sensory, motor, language, or visual areas of the cortex. Using *angiographic-volume* criteria (as previously described) [51,60,61], the preradiosurgical volumes of the malformations were 0.33-288 cm^3; 25% of AVMs were larger than 25 cm^3.

AOVMs

Intracranial vascular malformations that have clinically demonstrable effects yet are angiographically occult are readily imaged by MRI (and to a lesser extent, CT) [35,37]. AOVMs usually have a characteristic MRI appearance due to acute and chronic hemorrhage-associated changes [1,2]. We have found that these MRI findings generally have been predictive of an absence of abnormal vasculature on subsequent angiograms. Our preliminary results in patients with AOVMs treated with helium-ion radiosurgery have been reported elsewhere [37,68]. Between July 1983 and July 1989, we treated 35 patients with symptomatic AOVMs, 20 male and 15 female, ranging in age at the time of treatment from 13 to 64 years. Fourteen patients (40%) were in *excellent* grade prior to treatment, 17 (49%) in *good* grade, and 4 (11%) in *poor* grade. Nineteen AOVMs (54%) were located in the brain stem, 9 (26%) in the thalamus or internal capsule, 3 (9%) in the basal ganglia, 3 (9%) in the motor or language cortex, and 1 in the cerebellopontine angle. Using *treatment-volume* criteria, AOVMs measured between 0.1 cm^3 and 15.2 cm^3.

Clinical Follow-up and Outcome

About 150 patients have had a 48-month follow-up review, and 300 were followed up for 24 months. We now regularly extend follow-up to 9 years when feasible. Among the first 300 patients who were evaluated clinically to mid-1990, about 90% had an *excellent* or *good* neurologic clinical grade, about 5% had a *poor* clinical grade, and 5% had died of disease progression (including AVM hemorrhage) or unrelated intercurrent illness [11,12,13, 34,67]. Generally, a worsening of clinical grade has been due to intracranial hemorrhage or treatment-associated sequelae; these phenomena are described in detail in subsequent sections. A few patients have worsened from intercurrent medical disorders.

[TABLE 2 ABOUT HERE]

UCB-SUMC series

Clinical evaluation in our UCB-SUMC series of 86 patients, performed 24-72 months (mean, 38 months) after radiosurgery, found that 63% of patients presenting with seizures and 68% of patients presenting with headaches had improvement of these symptoms [67]. Of 11 patients presenting with progressive neurologic deficits unrelated to hemorrhage, there was improvement in 3 patients and stabilization of neurologic status in 6 patients [67]. Table 2 shows the clinical grade after radiosurgery for 101 consecutive patients (including 15 patients with AOVMs) as a function of preradiosurgical clinical grade. Clinical outcome was *excellent* in 58% and *good* in 36% of all patients in the series [67]. Generally, patients presenting initially in *excellent* or *good* condition did much better than those with a *poor* grade.

AOVMs

Clinical follow-up in 35 patients with AOVMs ranged from 1 to 7 years (mean, 40 months), including 31 patients followed up for more than 2 years [37,68]. Clinical follow-up grade was *excellent* in 46% of patients, *good* in 31%, *poor* in 14%; 3 patients (9%) were

dead [67]. Twenty-six patients in *excellent* or *good* condition prior to treatment remained stable or improved neurologically. Two patients initially in *poor* condition, who previously had received conventional radiotherapy, died of disease progression 9 and 14 months after treatment, and another patient initially in *good* condition died of recurrent hemorrhage. All three patients had been treated with radiosurgical doses ≤ 10 GyE. Seven other patients (20%) deteriorated neurologically due to recurrent AOVM hemorrhage 2 months to 5 years after treatment (four within 13 months). Four of these patients recovered fully to their previous condition, and three were permanently worse. Three patients subsequently underwent microsurgical resection of their AOVMs, 20 months, 3 years, and 5 years, respectively, after radiosurgery. At surgery, these AOVMs were found to be partially thrombosed, and this was confirmed histologically [68]. Four patients (11%) had apparently treatment-associated complications; these are described in a later section.

Neuroradiologic Response

Cerebral angiography was performed at yearly intervals to evaluate postradiosurgical changes in the vessels and pathologic shunts in the AVM. The first hemodynamic changes observed include a decrease in blood flow through the AVM, probably due to progressive obliteration of the small shunting vessels, with a decrease in size of the feeding arteries and draining veins. This stage is followed by a progressive decrease in the AVM volume until stabilization or complete obliteration of the AVM occurs.

Three years after radiosurgery, angiograpic studies in 230 patients demonstrated the following 3-year rates for complete obliteration as a function of *treatment volumes*: 90-95% for volumes <4 cm^3 (49% of the 230 patients), 90-95% for volumes between 4 cm^3 and 14 cm^3 (33% of patients), and 60-70% for volumes >14 cm^3 (18% of patients). For all volumes up to 70 cm^3, the rate has been approximately 80-85% (Figs. 10, 13, and 14) [11,13,34,67]. Following complete AVM obliteration, we have not seen angiographic reappearance of the malformation [13,34,67]. In patients who have been followed up with angiographic studies for longer than 36 months without complete obliteration, stabilization of the obliterative

process may have occurred, and it is probable that further changes in the hemodynamic condition or structure of the abnormal shunting vessels are not to be expected. MRI and CT scans are performed regularly to assess the delayed response of the brain parenchyma to the irradiation procedure; these findings are discussed later.

UCB-SUMC Series

The angiographic results 2 years after radiosurgery in the UCB-SUMC series (Table 3) indicate that complete obliteration of the AVM occurred in 70%, partial obliteration (10-99% obliteration) in 23%, and no change occurred in 7% [67]. By 3 years after treatment, 92% of patients had complete AVM obliteration, 4% had partial obliteration, and 4% experienced no change. The rate and extent of obliteration appear to be threshold phenomena directly related to the AVM volume and the radiation dose [67]. Smaller AVMs had higher rates of obliteration than larger ones ($p<0.005$ after 1 and 2 years, Mann-Whitney test). AVMs smaller than 4 cm^3 thrombosed more rapidly and more completely than larger lesions ($p<0.05$ for the comparison with AVMs 4 cm^3 to 25 cm^3 in volume and $p<0.001$ for the comparison with those >25 cm^3, Cox test) (Fig. 15). Intermediate-sized AVMs were obliterated more rapidly and more completely than large AVMs ($p<0.05$, Cox test).

[TABLE 3 ABOUT HERE]

Complete obliteration occurred more frequently in malformations treated with higher doses (30-45 GyE) ($p<0.05$ after 1 and 2 years, Mann-Whitney test) (Table 4) [67]. AVMs treated with intermediate doses (24-28 GyE) also responded well at 2 and 3 years. Preliminary results with the lowest-dose group (11.5-20 GyE) were encouraging after 3-year follow-up, but thus far the number of patients in this group is too small to permit firm conclusions.

[TABLE 4 ABOUT HERE]

AOVMs

Because it is not possible to follow the process of vascular obliteration in AOVMs using angiography, neuroradiologic follow-up used to evaluate the response of the AOVM and the adjacent brain tissue has been limited to sequential MRI and CT scans. Most patients demonstrated little change on MRI scans over time, other than what could be explained by partial resorption or evolution of pre-existing hemorrhage [37]. In several patients, findings of enhanced signal developed on T2-weighted MRI, but only one had concomitant clinical worsening, and this proved to be secondary to recurrent hemorrhage. We have found follow-up CT scanning to be of limited value, other than for diagnosing acute recurrent hemorrhage where clinically suspected [37].

Post-Treatment Hemorrhage

UCB-SUMC Series

Ten of 86 patients (12%) have hemorrhaged from residual angiographically demonstrable AVMs after radiosurgery, 7 patients during the first year, and 3 thereafter [67]. Hemorrhage resulted in permanent new neurologic deficits in 3 patients and death in 2 patients; the other 5 patients recovered fully. AVMs in 7 of these 10 patients had bled before treatment. No patients with angiographic evidence of complete obliteration of the malformation hemorrhaged subsequently. However, until complete obliteration occurs, patients with residual shunts remain at risk; one patient with 95% AVM obliteration bled 34 months after treatment [67].

Complications and Sequelae

Serious *early* sequelae have been negligible following stereotactic heavy charged-particle radiosurgery [34,36,67]. Generally, acute adverse effects have been limited to transient and readily controlled increased seizure activity in only a few patients who had a history of seizures. A few patients who presented initially with severe headaches have required increased doses of oral analgesics for a few days following treatment. No patients have

experienced nausea, vomiting or hyperpyrexia. No deaths have occurred from the irradiation procedure.

Several categories of *delayed* radiation injury have been observed [34,36,52,63]. On the basis of MRI, CT, angiography, and clinical evaluation, the treatment-associated sequelae can be classified as white matter changes or vasculopathy and include vasogenic edema, occlusion of functional arterial or venous vasculature, and radiation necrosis. The manifestations and incidence of clinical sequelae depend, in part, on the region of the brain involved, the volume of normal and abnormal brain tissue affected, the radiation dose, the presence of prior tissue injury from spontaneous hemorrhage or previous interventional procedures, and the timing and nature of therapeutic measures.

Asymptomatic Vasogenic Edema

Vasogenic edema presents most commonly as an asymptomatic occurrence, initially appearing on MRI studies required during routine follow-up. Radiographically, the edema is seen in the immediate region of the AVM as high-intensity signal on T2-weighted MRI or as a region of low attenuation on CT images [34,36,63,67]. Some MRI changes consistent with vasogenic edema have been found to develop primarily in the irradiated deep white matter in almost half of patients whose AVMs were treated with higher-dose (>25 GyE) helium-ion radiosurgery [63,67]. This process is much more common when the treatment volume is located deep within the substance of the central white matter and appears to be a consequence of the relatively loose cellular packing in the white matter that permits diffusion of fluid into surrounding tissue. Its underlying etiologic process is poorly understood but seems to be associated with delayed radiation-induced injury of the vascular endothelium of the smaller shunts, with loss of integrity of the intimal boundary and with concomitant plasma transudation into the brain parenchyma [63]. Most often the process is contained, limited to the immediate 2- to 3-mm shell surrounding the irradiated target volume, and the patient remains asymptomatic; the process is always limited to the irradiated hemisphere. Even extensive regions of white matter edema may be present without clini-

cal manifestations (Figs. 16 and 17). This edema usually is observed about 12-18 months after treatment and may persist with limited effects or extend over the next 12-24 months and then undergo spontaneous regression without treatment [34,36,52,63]. Sequential MRI studies in asymptomatic patients show that complete regression to normal or near-normal brain architecture occurs up to 36 months following treatment (Fig. 17).

[NOTE: FIGURES 16 AND 17 SHOULD BE ADJACENT OR 16 ABOVE 17]

Symptomatic Vasogenic Edema

Where edema is extensive or involves central brain loci, the associated mass effect can cause reversible or irreversible brain injury associated with neurologic dysfunction (Fig. 18) [34,36,52,63]. Symptomatic delayed vasogenic edema developed in as many as 12-14% of our radiosurgical patients, but about half were only minimally or transiently symptomatic, and most responded quickly to prompt corticosteroid therapy. While the edema process is dose-dependent and volume-dependent, the clinical symptoms and their progression depend in large measure on the site in which the changes occur. The condition occurred most often in patients treated in the initial phases of our dose-searching protocols, usually with doses in the range of 35-45 GyE. No cases of symptomatic vasogenic edema have occurred in patients treated with doses less than 25 GyE [34,36,52,63,67].

Radiation Necrosis

Histologically confirmed, symptomatic, delayed radiation necrosis has occurred in about 2-3% of our patients after total radiation doses of 25-45 GyE delivered in a single session or two daily fractions (Fig. 19). However, other cases of necrosis probably have been masked in some patients with vasogenic edema who are clinically asymptomatic, because the focal injury was limited to a relatively small and silent region of the brain, or in patients in the *symptomatic vasogenic edema* group who responded variably to corticosteroids (Fig. 20). In general, the timing and extent of radiation necrosis largely depends on the radiation dose and volume of brain treated, but severe radiation injury of the brain parenchyma can occur

at doses below 32 GyE, that is, well below the range of 35-45 GyE initially studied in the dose-searching protocol. The extent to which the injury is manifested clinically depends uniquely on the region of the brain affected and the volume of damaged tissue involved. Currently, brain necrosis has not been observed in patients treated with doses of 25 GyE or less, even when relatively large volumes of brain tissue are irradiated [67].

Arterial Occlusion

Though uncommon, occlusion of functional arterial vessels resulting from radiation-induced vasculopathy immediately adjacent to, or within, the AVM and associated with regional cerebral infarction can be a more serious clinical problem than vasogenic edema [34, 36,52,63,67]. Radiosurgery generally causes obliteration of abnormal arterial and arteriolar shunts within the AVM, but the normal arterial vasculature, though occasionally irradiated with relatively high doses, appears to be considerably more resistant to the degenerative and subsequent obliterative changes [63]. The presence of collateral circulation can prevent this complication from becoming symptomatic more frequently than clinically observed; serious consequences occur in only 2-3% of patients.

Symptomatic arterial vasculopathy and occlusion has occurred as early as 8 months and as late as 27 months following radiosurgery [36,52,63,67]; the process is dose-dependent and volume-dependent. Most often it is mild and transient in its clinical manifestations, generally associated with the development of neurologic dysfunction related to the region of vascular embarrassment. MRI and CT typically do not demonstrate signs of regional edema [36,52,63]. In some cases, angiography may confirm complete obliteration of the AVM and fail to reveal evidence of vasculopathy; subacute small-vessel occlusion is considered to be the mechanism of injury (Fig. 21) [34,36,63]. Major neurologic dysfunction can occur if a major artery is occluded and no collateral circulation is available. Three of our patients had angiographically demonstrable vasculopathy with concomitant infarction and mild to severe neurologic deficit (Fig. 22) [34,36,63,67].

Venous Thrombosis

Thrombosis of venous outflow tracts that drain AVMs appears to occur rarely following charged-particle radiosurgery, perhaps because veins are much less sensitive than arteries to the effects of radiation [20]. The venous component is believed to represent a passive sink, even in high-volume, high-flow AVMs, and complete obliteration of all the pathologic shunts in the malformation can be achieved without including the venous component in the radiation field. Additionally, obstruction of the venous outflow tract is undesirable because of the risk of causing venous infarction. Therefore, treatment planning for charged-particle radiosurgery takes into account the initial venous phase on angiography and is designed to exclude from the radiation beams, to the extent possible, the larger venous structures of the AVM. Clinically, patients are often asymptomatic and do not show radiographic evidence of edema.

Aneurysms

None of our patients with AVMs have hemorrhaged from a previously treated aneurysm. However, two patients have hemorrhaged from untreated aneurysms a number of months following charge-particle radiosurgery. One patient hemorrhaged from an aneurysm of the basilar artery tip 10 months after radiosurgery was performed for a large left parietal AVM. The aneurysm was not present on the angiograms obtained prior to treatment (Fig. 23) and did not rupture until there was almost complete obliteration of the AVM (Fig. 24). We believe that obliteration of the high-volume, high-flow AVM led to increased regional intravascular resistance and pressure gradients, which were transmitted to the vertebral artery branches and the basilar artery. These hemodynamic alterations were sufficient to induce expansion and bleeding from a dormant, but potentially lethal, remote arterial aneurysm. The aneurysm was treated by surgical clipping, the patient made an excellent recovery, and the treated AVM obliterated completely within the next several months without further sequelae [36,63].

[NOTE: FIGS. 23 AND 24 SHOULD BE SIDE-TO-SIDE (COMBINED 10 FRAME

SEQUENCE)]

UCB-SUMC Series

In our UCB-SUMC series recently analyzed, clinical complications following radiosurgery were most common in patients with AVMs in the brain stem, thalamus, or basal ganglia [67]. About 20% of patients (17 of 86) experienced complications between 3 and 38 months after treatment (mean, 13.4 months). Seven patients had minor complications, such as visual field deficit, diplopia, unilateral hearing impairment, slight gait ataxia, or mild paresis; three of them recovered completely and four, partially. Ten patients (12%) had major complications, including hemiparesis, gait ataxia, cranial nerve palsies, partial aphasia, or hypothalamic syndrome; two recovered fully, seven recovered partially, and one remained unchanged. Some patients had more than one complication. Hemiparesis was the most common major complication and visual field deficit was the most common minor complication.

In about half of all the patients (33 of 65) examined after radiosurgery with MRI and CT, deep-white-matter changes occurred between 4 and 26 months after treatment (mean, 15.3 months); 20 of these patients were asymptomatic. In the 13 patients who were clinically symptomatic, the white-matter changes had MRI and CT patterns consistent with those described following radiation-induced brain injury, viz., abnormal signals on MRI or low attenuation on CT scans. These findings usually were associated with an appreciable amount of cerebral edema. In this series, a biopsy of the involved white matter in one patient revealed areas of tissue necrosis. In two symptomatic patients, the changes observed on MRI and CT resolved completely, and in 11 patients, partially.

Radiation-induced vasculopathy occurred in three patients and was characterized by arterial stenosis or thrombosis on cerebral angiograms and by MRI and CT changes consistent with cerebral ischemia. The radiation doses ranged from 25-45 GyE, delivered to *angiographic volumes* of brain tissue of 0.85 cm^3 to 40 cm^3. Complications were more prevalent with higher doses and larger volumes of treated brain tissue (Fig. 25) [67]. Among the 20 patients who received doses above 25 GyE and whose angiographic volumes of treated tissue

were more than 13 cm^3, 10 experienced major or minor complications; these represented almost 60% of all clinical complications. All complications occurred among the initial 46 patients treated in the higher-dose phase of the dose-searching protocol. None of the 40 patients in the series treated with lower doses in the later phases of the protocol experienced any complications during this last 5-year period since 1986 [67].

AOVMs

Four of 35 patients (11%) with AOVMs had apparently treatment-associated sequelae 3 to 12 months after helium-ion radiosurgery, although only one patient had findings of enhanced signal on T2-weighted MRI. Three of these patients made a complete recovery, and one had permanent worsening. More than one cause may have contributed to neurologic deterioration in some of these patients, such as undetected recurrent hemorrhage or thrombosis combined with radiation effects.

Other Clinical Observations

Additional Therapy

In selected patients in whom heavy charged-particle radiosurgery has not achieved complete AVM obliteration within 3 years, we have carried out additional treatment with microsurgery, embolization, or both. In three patients who underwent open surgery for residual AVMs several years after radiosurgery, we found the AVMs to be markedly less vascular and more easily resected than expected had the patient not received radiosurgery. In another patient whose AVM was not obliterated 3 years following radiosurgical treatment, we were able to achieve complete thrombosis of the AVM using endovascular embolization alone. It appears that the small-vessel component likely had been obliterated by the radiation treatment, and that embolization-induced occlusion of the limnited number of residual fistulae was able to obliterate fully the remaining AVM shunts. Although our experience with helium-ion radiosurgery prior to open microsurgery and embolization is limited, this

approach may prove useful in the multistage management of some unusually large and complex AVMs in which complete obliteration has not occurred by 3 years or more.

Partial-Volume Radiosurgery

Certain sequelae of the treatment procedure may arise from the hemodynamic alterations of the AVM as it undergoes obliteration [36,38]. The creation of high-flow shunting within the AVM may increase the probability of intracranial hemorrhage. This is a potential hazard of any incomplete treatment. Undesirable shunts can be created acutely, by subtotal surgical excision or embolization, or subacutely, by limited focal irradiation (*partial-volume radiosurgery*) [38].

During the initial phase of our clinical protocol, a selected number of patients with large hemispheric AVMs were treated with stereotactic focal irradiation solely to the earliest-filling component of the arterial phase, that is, the so-called *nidus* of the AVM, rather than the entire angiographic arterial phase, that is, the complete AVM *core* (Fig. 26). Such partial-volume irradiation resulted in effective obliteration of the precisely defined therapeutic target only, and generally without any complications. However, the periphery of the malformation was left intact, thereby creating an undesirable shunt with some high-volume, high-flow characteristics and with attendant risks of hemorrhage. We no longer consider it acceptable to treat any AVM without encompassing its entire arterial phase with a homogeneous dose distribution. Those patients whose initial radiosurgical treatment failed to meet these criteria are re-evaluated and given additional treatment if any residual shunts of the AVM persist.

OTHER CLINICAL SERIES

Stereotactic charged-particle radiosurgery has been used to treat intracranial vascular malformations in approximately 2,000 patients worldwide since 1965 (Table 5). Our experience with heavy charged-particle (helium-ion) radiosurgery has been paralleled by extensive experience with proton-beam therapy at the Harvard Cyclotron Laboratory-Massachusetts

General Hospital (HCL-MGH) [23,24,25,26,27,28], the Burdenko Neurosurgical Institute-Institute for Theoretical and Experimental Physics (BNI-ITEP) in Moscow [56,57,58], and the Leningrad Institute of Nuclear Physics (LINPh) [29,55]. At all three centers, individually designed treatment plans are developed for every patient and multiport stereotactically directed beam-delivery procedures are used to achieve uniform dose localization and dose distribution. All radiosurgical treatment planning use RBE values of approximately 1.0 for the proton plateau and Bragg-peak ionization regions.

[TABLE 5 ABOUT HERE]

Kjellberg and associates [23,24,25,26,27,28] have used single-fraction Bragg-peak proton (160 MeV) therapy at HCL-MGH to treat more than 1300 patients with vascular malformations of the brain, including 98 patients with AOVMs (Kjellberg RN, personal communication, October 1989). An immobilizing frame, fixed to the patient's skull with drill rods, has been developed for stereotactic proton therapy. Irradiation generally is delivered with parallel opposed treatment fields. Doses are selected according to diameter of the AVM, using a nomogram based on dose, volume, and complication rate in a large number of treated patients [27].

Findings of follow-up evaluation in 1000 patients with AVMs, 2 to 24 years after treatment with proton-beam therapy, recently were reported [25]. In 104 patients, the the clinical outcome was unrelated to hemorrhage or proton-beam therapy. Of the remaining 896 patients, 818 (91.3%) were the same or improved as compared to their neurologic status at the time of treatment; 27 (3%) had moderate deficits from hemorrhage or proton-beam therapy but functioned independently at pretreatment levels; 7 (0.8%) had severe deficits and were dependent to varying degrees; 2 (0.2%) were vegetative; 39 (4.4%) were dead (37 from hemorrhage and 2 from treatment complications); 3 (0.3%) were lost to follow-up after surviving hemorrhage [25]. Analysis by actuarial life-table methods showed 98.4% 24-year survival for patients with AVMs ≤3 cm in diameter and 93% 24-year survival for all patients [25]; these data were compared to the 77% 24-year survival reported for an untreated control

group [6]. Of the 37 patients who died from hemorrhage, 22 died within the first 2 years after treatment; 33 lethal hemorrhages occurred in patients with AVMs >3 cm in diameter. An additional 101 patients survived hemorrhage, including the 3 above-mentioned patients who were lost to follow-up. Complications of treatment occurred in 17 patients (6 months to 6.5 years after treatment), but only 7 were in the last 925 patients following downward adjustments in treatment doses [25].

Minakova and colleagues [56,57,58] have used Bragg peak proton radiosurgery at BNI-ITEP in a series of 66 patients with AVMs and 24 patients with cavernous-carotid fistulae (Minakova YeI, personal communication, October 1990). In their method, patient immobilization for AVM radiosurgery is accomplished by use of a thermoplastic-mask system. The Bragg peak is spread to a width of 15-25 mm as required; seven or eight beam ports are used. Single-fraction maximum doses of 30-50 Gy are used, depending on the size and location of the AVM; the periphery of the lesion is treated to the 50% isodose. Of 28 patients followed up angiographically for 2 years after treatment, 71% demonstrated total or partial obliteration. Two patients sustained hemorrhage within the first year after treatment. Two patients experienced neurologic sequelae with corresponding CT findings of edema, the onset occurring in one patient at 22 months, and in the other, 18 months after radiosurgery (dose, 50 Gy; beam diameter, 20 mm). Both patients responded well to brief courses of high-dose steroids. For radiosurgery of carotid-cavernous fistulae, the Moscow group achieves patient immobilization via bone-studs in cranial structures and *through-and-through* plateau-beam irradiation is used for treatment (10- to 12-mm beams, 1 or 2 fractions, 40- to 60-Gy dose). Thus far, all patients have had regression of ocular symptoms and headaches, usually between 4 and 8 months after treatment. In four of eight patients. complete obliteration was observed on follow-up angiograms; no patient experienced adverse sequelae (Minakova YeI, personal communication, October 1990).

Konnov and co-workers [29,55] have used only the plateau portion of the proton beam (1000 MeV) at the LINPh to treat 187 patients with AVMs and 6 patients with arterial

aneurysms (Konnov BA, personal communication, February 1990). A head-immobilization system was developed using individualized thermoplastic masks supplemented by metal markers inserted bilaterally into the lateral aspect of the skull [55]. Prior to proton therapy for AVMs, intravascular embolization was performed in 18 patients, and partial surgical excision in 16 patients of the first 148 patients treated. Using isocentrically directed converging irradiation arcs, maximal doses of 40-80 Gy were delivered to diameters of 5-10 mm; the irradiated-field size was defined by the extent of the 50% isodose contour [29]. Larger AVMs were treated with two isocenters. Five patients died from recurrent hemorrhage during the first year. Angiographic follow-up for 1 to 8 years after treatment was obtained in 109 patients. Complete AVM obliteration was achieved in 23 of 36 patients (64%) with angiographically determined AVM volumes ≤ 2.0 cm^3, in 7 of 20 patients (35%) with 2.1-4.0-cm^3 AVMs, in 3 of 10 (30%) with 4.1- to 6.0-cm^3 AVMs, and in 1 of 43 (2%) with AVMs >6.0 cm^3 [55]. Nearly all cases of complete AVM obliteration occurred within the first 3 years after treatment. AVM obliteration and volume decrease were positively correlated with both average absorbed dose and dose to the margin of the treatment volume [55]. (The dose distributions achieved with the use of isocentrically directed arcs of plateau-beam irradiation [rather than the Bragg peak method] are quite comparable to those produced with stereotactic radiosurgical systems using x-rays or gamma rays. Therefore, they would be expected to be similarly limited in their application to large lesions. The reader is referred to our recent report in *Neurosurgery Clinics of North America* for a detailed discussion of plateau-beam irradiation of intracranial targets [35].)

DISCUSSION

The prognosis for patients with symptomatic, untreated AVMs in deep or critical locations in the brain is poor, and 40-80% of patients with such malformations become severely disabled or die of their disease at a relatively early age [17,18,19,66]. The risks of conventional surgery for these difficult lesions are extremely high, the combined morbidity and

mortality exceeding 20-30% [7,8,19,30,64]. Alternative interventional procedures, such as cryosurgery, electrothermal surgery, and conventional radiotherapy, provide poor spatial definition and lack reliability in confining the reaction to injury of the brain tissues [4]. We have found that stereotactic heavy charged-particle radiosurgery obliterates high-flow AVMs and protects against further brain hemorrhage with reduced morbidity and no treatment-related mortality. In our series, an *excellent* or *good* neurologic grade resulted in 94% of AVM patients. These radiosurgical results must be considered in relation to the natural history of such pernicious lesions and the results of conventional neurosurgical approaches. The current procedure still has two major disadvantages: the prolonged latent period (up to 3 years) and the incidence of serious neurologic complications (about 11%). At present we consider the radiosurgical procedure only for selected symptomatic patients with intracranial AVMs in whom the conventional surgical risk is considered unacceptably high, and patient selection criteria remain constrained by specifically defined multi-institutional patient protocols.

The clinical objectives of stereotactic radiosurgery for the treatment of intracranial AVMs are to achieve changes in the intracerebral hemodynamic condition, resulting in (1) reduction or elimination of intracranial hemorrhage and its associated morbidity and mortality, (2) improved clinical outcomes associated with decrease in progressive or fixed neurologic deficits, (3) lower frequency of seizures, and (4) fewer subjective complaints, including frequency and intensity of disabling headaches [10,34,67]. In order to achieve these objectives optimally, the entire AVM must be obliterated and the hemodynamic condition converted to normal or near-normal cerebral perfusion characteristics insofar as possible. We now know that the biologic basis for this change in the abnormal vasculature involves radiation-induced injury to the endothelial cells and intimal proliferation and hyaline degeneration of the media, thereby establishing favorable conditions for blood coagulation and progressive thrombosis [20]. Highly localized charged-particle beam irradiation of the intracranial AVM has been shown to produce progressive thrombosis of the abnormal blood

vessels. The thrombotic process begins to appear after some 3-6 months, and typicallly requires 12-36 months for complete vascular obliteration to occur [10,14,15,34,67]. Complete obliteration of the AVM, while reducing the potential for treatment-associated complications to the lowest possible level, is the therapeutic goal for all patients. The mechanisms underlying the observed improvements in seizure activity and headache syndromes and the stabilization or improvement of progressive nonhemorrhagic neurologic dysfunction are poorly understood. However, these changes appear to be associated, in large measure, with the improved rCBF, stabilization of hemodynamic imbalance, and reversal of vascular steal associated with progressive thrombosis of the malformation (Figs. 10 and 14) [65,67].

Because the presence of arteriovenous shunts is associated with hemorrhage, patients remain at risk until the malformation is completely obliterated. The data are too sparse at present to determine whether any degree of protection against hemorrhage is conferred during the prolonged latency period before complete obliteration or by incomplete obliteration. We have hypothesized that partial thrombosis or narrowing of the vascular shunts is accompanied by an increase in intravascular outflow-resistance in the remaining patent shunts, thereby predisposing the AVM compartment to hemorrhage before obliteration is complete [38]; our preliminary clinical observations appear to support this hypothesis, but further study is required. Suboptimal irradiation can result as a consequence of inadequate cerebral angiography, application of multi-isocenter contouring to large and irregular target volumes, or attempting to define the complete anatomical core of an AVM without a full understanding of the pathologic architecture.

The exceptional precision with which stereotactically directed charged-particle beams can be used for focal irradiation has made possible a better understanding of the mechanisms of radiation-induced injury in normal brain tissues [63]. However, the tissue immediately surrounding an AVM or intertwined with it quite often cannot be considered as normal. These regions may have been subject to previous hemorrhagic, surgical or embolic insults. Impaired local perfusion with a concomitant vascular steal phenomenon is

commonly present, with considerable dimunition of oxygenation and nutrition to the regional brain tissue and accumulation of metabolic waste products (Figs. 10, 14, and 23) [10,14,15,54,63].

AOVMs

It is recognized that clinically symptomatic AOVMs comprise a number of pathologic conditions, and only about half of these may be architecturally similar to AVMs that are angiographically demonstrable [40]. Accordingly, mechanisms of thrombotic vascular obliteration that are associated with radiation-mediated vascular injury in the brain may not apply in all cases of AOVMs. In the absence of established neuroradiologic criteria for differentiating the various types of AOVMs, we have chosen to enter patients into the treatment protocol based on their clinical status and symptoms in addition to neuroradiologic evidence of prior hemorrhage. Furthermore, current neuroradiologic techniques are not sufficiently sensitive for imaging the obliterative response in the vascular shunts of these slow-flow AOVMs. Therefore, we have reported the clinical outcomes separately from those of the angiographically demonstrable AVMs and based on the long-term clinical and MRI follow-up required to assess the response to heavy charged-particle radiosurgery [34,35,37,67].

The clinical results following helium-ion radiosurgery for AOVMs are not as favorable as our results with high-flow AVMs. However, it may be that symptomatic, deep-seated AOVMs have a particularly poor natural history, in part due to their critical location [1]. We believe that microsurgical resection should be the primary treatment for surgically accessible, symptomatic AOVMs. To assess the potential value of helium-ion radiosurgery for surgically inaccessible AOVMs, the natural history of these lesions must be better defined, and a larger number of treated patients must be followed up over longer periods. Recent developments in MRI of flow dynamics may provide methods to differentiate lesions that are true AVMs and those that are other types of occult vascular malformations, such as cavernous angiomas. Improved diagnostic specificity should provide improved criteria for patient selection for stereotactic radiosurgery and should aid in image correlation for

treatment planning and long-term evaluation of clinical and neuroradiologic response to treatment [34,35,37,67].

CURRENT RESEARCH AND FUTURE DIRECTIONS

Despite the high AVM-obliteration rate, improvement in clinical symptoms, and relatively low incidence of major complications, our current clinical research efforts continue to be directed toward improving cure rates for larger and more complex vascular malformations and investigating mechanisms of late radiation-induced injury to decrease the incidence of delayed complications and influence treatment strategies. Our dose-searching protocols investigate treatment variables, including optimal dose, fractionation, and malformation size and location. Although our dose-reduction protocol, which currently brackets a range of 15-25 GyE, has lowered the incidence of delayed complications, it also may lead to undesirable clinical outcomes by decreasing the incidence of complete AVM obliteration or extending the latency interval until complete obliteration. This appears particularly the case in the treatment of large and complexly shaped AVMs. By attempting to eliminate all potential risks of late complications, patients may be placed at increased risk of morbidity or mortality due to post-treatment hemorrhage.

An increasing number of patients are now evaluated for multistage procedures, including flow-directed endovascular embolization and partial surgical resection in selected cases, to reduce malformation size and decrease the high rate of blood flow in preparation for radiosurgery. Although this approach is proving useful for certain large and complex malformations, the potential for serious complications associated with partial surgical resection and/or endovascular embolization has been recognized [67]. Consequently, these adjunctive procedures currently are recommended prior to radiosurgery only under special circumstances, such as for unusually large hemispheric AVMs with high-flow, high-volume perfusion characteristics. However, these are the AVMs associated with the poorest rate of complete obliteration and with the highest incidence of late complications.

We presently are carrying out a number of clinical trials aimed at achieving a better understanding of the hemodynamic and morphologic changes following radiosurgery, particularly in high-volume, high-flow malformations. These include (1) investigation of the mechanisms of demyelination and repair associated with delayed radiation-induced injury in the brain, including transient or permanent disturbances in BBB integrity and fluid balance; and (2) evaluation of rCBF and alterations in the size of arterial feeders, shunts, and draining veins, associated with progressive obliteration of the malformation and normalization of regional blood flow [34,36,63].

MRI studies presently in progress are designed to detect early and late cerebrovascular effects of focal, heavy charged-particle irradiation in relation to radiation dose, dose-fractionation, and volume of irradiated tissue, and to correlate these changes with those defined by PET scanning (Figs. 20 and 27). These studies assess the prognostic significance of changes seen with MRI and PET and attempt to determine the relationship of these changes to the brain's reaction to radiation-induced injury [39]. MRI is also an essential component of image-correlation procedures, involving CT, cerebral angiography, and PET, particularly related to the development of three-dimensional conformal treatment planning for charged-particle radiosurgery. PET scanning studies are performed in selected patients to determine brain tissue tolerance and repair to help elucidate the pathophysiologic mechanisms and metabolic significance of the radiation-induced changes observed on MRI, and to demonstrate cerebral AVM structure and function in relation to altered rCBF dynamics (Figs. 20 and 27) [73]. PET studies with ^{82}rubidium evaluate BBB integrity; vascular ^{82}Rb is rapidly cleared from the brain, and the PET image represents tracer activity that has crossed the BBB into the brain parenchyma. PET studies using ^{18}fluorodeoxyglucose examine cellular deoxyglucose uptake and trapping, an accurate measure of glucose metabolic activity in the normal and irradiated brain. ^{122}I-HIPDM evaluates rCBF dynamics. It has been shown that decreased ^{18}FDG uptake occurs in the presence of radiation necrosis, but it is not known how early after radiation injury this effect is quantifiable or whether such early

changes can be used as a predictive index for modifying therapeutic strategies (Fig. 20) [73]. Radiation necrosis is accompanied by decreased rCBF perfusion, but the stage of injury at which this decrease is first measured and the specificity of this observation are not yet fully understood. Late radiation-induced injury in the brain results in massive BBB breakdown, but compromised BBB integrity also accompanies less serious, subclinical radiation damage (Fig. 17).

Patients with intracranial AVMs are being studied using stable-xenon-enhanced CT to examine the temporal pattern of tissue response and rCBF following heavy charged-particle radiosurgery (Fig. 28) [54]. High-volume, high-flow rCBF dynamics can cause neurologic dysfunction by the vascular steal phenomenon, in which tissue perfusion is decreased in the brain tissues adjacent to an AVM (Figs. 10, 14, and 23). Xenon-CT studies provide a detailed map for quantifying altered rCBF in brain tissue adjacent to and remote from the vascular malformation (Fig. 28). Reduction in blood flow can occur in both cerebral hemispheres and is most severe when the malformation is large or has a major intracranial arterial supply; the effects are most pronounced in the adjacent brain tissues. It has been demonstrated that, following partial or complete vascular obliteration of the pathologic shunts, blood flow in adjacent and remote brain tissue increases. This process frequently is associated with stabilization or improvement of neurologic dysfunction and a decrease in the frequency and intensity of seizures and vascular headaches [10,67].

SUMMARY

Heavy charged-particle radiation has unique physical characteristic that offer several advantages over photons and protons for stereotactic radiosurgery of intracranial AVMs. These include improved dose distributions with depth in tissue, small angle of lateral scattering, and sharp distal fall-off of dose in the Bragg ionization peak. Under multi-institutionally approved clinical trials, we have used stereotactic helium-ion Bragg peak radiosurgery to treat approximately 400 patients with symptomatic, surgically inaccessible vascular mal-

formations at the UCB-LBL 184-inch synchrocyclotron and Bevatron. Treatment planning for stereotactic heavy charged-particle radiosurgery for intracranial vascular disorders integrates anatomic and physical information from the stereotactic cerebral angiogram and stereotactic CT and MRI scans for each patient, using computerized treatment-planning calculations for optimal isodose contour distribution. The shape of an intracranial AVM is associated strongly with its treatability and potential clinical outcome. In this respect, heavy charged-particle radiosurgery has distinct advantages over other radiosurgical methods; the unique physical properties allow the shaping of individual beams to encompass the contours of large and complexly shaped AVMs, while sparing important adjacent neural structures.

We have had a long-term dose-searching clinical protocol in collaboration with SUMC and UCSF and have followed up over 300 patients for more than 2 years. Initially, treatment doses ranged from 45 GyE to 35 GyE. Currently, total doses up to 25 GyE are delivered to treatment volumes ranging from 0.1 cm^3 to 70 cm^3. This represents a relatively homogeneous dose distribution with the 90% isodose surface contoured to the periphery of the lesion; there is considerable protection of normal adjacent brain tissues, and most of the brain receives no radiation exposure. Dose selection depends on the volume, shape, and location of the AVM and several other factors, including the volume of normal brain that must be traversed by the plateau portion of the charged-particle beam.

The first 230 patients have been evaluated clinically to the end of 1989. Using the clinical grading of Drake [7,8], about 90% of the patients had an *excellent* or *good* neurologic grade, about 5% had a *poor* grade, and about 5% had progression of disease and died, or died as a result of unrelated intercurrent illness. Neuroradiologic follow-up to the end of 1989 indicated the following rates of complete angiographic obliteration 3 years after treatment: 90-95% for AVM treatment volumes <4 cm^3, 90-95% for volumes 4 cm^3 to 14 cm^3, and 60-70% for volumes >14 cm^3. For all volumes (up to 70 cm^3), the rate of complete obliteration was approximately 80-85%. The rate and extent of AVM obliteration is a

threshold phenomenon directly related to treatment volume and dose. Protection against hemorrhage results only after complete obliteration of all pathologic shunts. The rate of serious complications, including symptomatic vasogenic edema (white-matter changes) and vasculopathy, is about 11%, but these were confined almost completely to the high-dose treatment group. No complications have occurred thus far in patients who received doses less than 25 GyE.

Until defined protocols establish common measurable variables and grading systems for neurologic and neuroradiologic studies, it will be difficult to make meaningful comparisons of the therapeutic results and related health outcomes in the few large clinical series for which they are available [24,67,69]. Given the natural history of these lesions, we conclude that heavy charged-particle Bragg peak radiosurgery is an effective treatment for symptomatic, surgically inaccessible intracranial AVMs. The current procedure has two disadvantages: the prolonged latency interval before complete obliteration of the vascular lesion and the risk of serious neurologic complications [67].

ACKNOWLEDGMENTS

References

[1] Abe M, Kjellberg RN, Adams RD: Clinical presentations of vascular malformations of the brain stem: comparison of angiographically positive and negative types. J Neurol Neurosurg Psychiatry 52:167–175, 1989

[2] Atlas SW: Intracranial vascular malformations and aneurysms. Current imaging applications. Radiol Clin North Am 26:821–837, 1988

[3] Blakely EA, Ngo FQH, Curtis SB, et al: Heavy-ion radiobiology: Cellular studies. *In* Lett JT (ed): Advances in Radiation Biology (vol 11). New York, Academic Press, 1984, pp 295–389

[4] Carrea R, LeVay D (eds): Neurological Surgery with Emphasis on Non-Invasive Methods of Diagnosis and Treatment. Amsterdam, Excerpta Medica, 1978

[5] Cox DR: Regression models and life-tables. J R Stat Soc [B] 34:187–220, 1972

[6] Crawford PM, West CR, Chadwick DW, et al: Arteriovenous malformations of the brain: J Neurol Neurosurg Psychiatry 49:1–10, 1986

[7] Drake CG: Cerebral arteriovenous malformations: Considerations for and experience with surgical treatment in 166 cases. Clin Neurosurg 26:145–208, 1979

[8] Drake CG, Friedman AH, Peerless SJ: Posterior fossa arteriovenous malformations. J Neurosurg 64:1–10, 1986

[9] Fabrikant JI, Budinger TF, Tobias CA, et al: Focal lesions in the central nervous system. *In* Pirruccello MC, Tobias CA (eds): Biological and Medical Research with Accelerated Heavy Ions at the Bevalac, 1977-1980. (LBL Report No. 11220). Berkeley, Regents of the University of California, 1980, pp 399–405

[10] Fabrikant JI, Frankel KA, Phillips MH, et al: Stereotactic heavy charged-particle Bragg peak radiosurgery for intracranial arteriovenous malformations. *In* Edwards

MSB, Hoffman HJ (eds): Cerebral Vascular Disease in Children and Adolescents, Baltimore, Williams & Wilkins, 1989, pp 389–409

[11] Fabrikant JI, Levy RP, Frankel KA, et al: Stereotactic helium-ion radiosurgery for the treatment of intracranial vascular malformations. *In* Proceedings of the International Workshop on Proton and Narrow Photon Beam Therapy, Oulu, Finland, 1989, pp 33–37

[12] Fabrikant JI, Levy RP, Phillips MH, et al: Neurosurgical applications of ion beams. Nucl Instrum Methods Phys Res B40/41:1376–1384, 1989

[13] Fabrikant JI, Levy RP, Steinberg GK, et al: Heavy-charged-particle radiosurgery for intracranial vascular disorders: Clinical results of 350 patients. *In* Proceedings of the European Particle Accelerator Conference, Nice, France, 1990, pp S61-S63

[14] Fabrikant JI, Lyman JT, Frankel KA: Heavy charged-particle Bragg peak radiosurgery for intracranial vascular disorders. Radiat Res [Suppl] 104:S244-S258, 1985

[15] Fabrikant JI, Lyman JT, Hosobuchi Y: Stereotactic heavy-ion Bragg peak radiosurgery: Method for treatment of deep arteriovenous malformations. Br J Radiol 57:479–490, 1984

[16] Fabrikant JI, Lyman JT, Hosobuchi Y: Stereotactic heavy-ion Bragg peak radiosurgery for intracranial vascular disorders. *In* Wilkins RH, Rengachary SS (eds): Neurosurgery, New York, McGraw-Hill, 1985, pp 1128–1132

[17] Fults D, Kelly DL Jr: Natural history of arteriovenous malformations of the brain: A clinical study. Neurosurgery 15:658–662, 1984

[18] Heros RC, Korosue K: Radiation treatment of cerebral arteriovenous malformations. N Engl J Med 323:127–129, 1990

[19] Heros RC, Tu Y-K: Is surgical therapy needed for unruptured arteriovenous malformations? Neurology 37:279–286, 1987

[20] Hopewell JW: Radiation effects on vascular tissue. *In* Potten CS, Hendry JH (eds): Cytotoxic Insult to Tissue. Edinburgh, Churchill Livingstone, 1983, pp 228–257

[21] Kaplan EL, Meier P: Nonparametric estimation from incomplete observations. J Am Stat Assoc 53:457–481, 1958

[22] Kessler ML: Integration of multimodality imaging data for radiotherapy treatment planning. Ph.D. Thesis, Berkeley, University of California, 1989

[23] Kjellberg RN: Stereotactic Bragg peak proton beam radiosurgery for cerebral arteriovenous malformations. Ann Clin Res 18 [Suppl 47]:17–19, 1986

[24] Kjellberg RN: Proton beam therapy for arteriovenous malformation of the brain. *In* Schmidek HH, Sweet WH (eds): Operative Neurosurgical Techniques (vol. 1), New York, Grune & Stratton, 1988, pp 911–915

[25] Kjellberg RN, Candia GJ: Stereotactic proton beam therapy for cerebral AVMs. *Harvard Radiosurgery Update*, Harvard Medical School, Chestnut Hill, MA, 1990 (abstract)

[26] Kjellberg RN, Davis KR, Lyons SL, et al: Bragg peak proton beam therapy for arteriovenous malformations of the brain. Clin Neurosurg 31:248–290, 1984

[27] Kjellberg RN, Hanamura T, Davis KR, et al: Bragg-peak proton-beam therapy for arteriovenous malformations of the brain. N Engl J Med 309:269–274, 1983

[28] Kjellberg RN, Poletti CE, Roberson GH, et al: Bragg-peak proton treatment of arteriovenous malformations of the brain. *In* Carrea R, LeVav D (eds): Neurological Surgery with Emphasis on Non-Invasive Methods of Diagnosis and Treatment. Amsterdam, Excerpta Medica, 1978, pp 181–187

[29] Konnov B, Melnikov L, Zargarova O, et al: Narrow proton beam therapy for intracranial lesions. *In* Proceedings of the International Workshop on Proton and Narrow Photon Beam Therapy, Oulu, Finland, 1989, pp 48–55

[30] Kunc Z: Deep-seated arteriovenous malformations: A critical review. *In* Carrea R, LeVay D (eds): Neurological Surgery with Emphasis on Non-Invasive Methods of Diagnosis and Treatment. Amsterdam, Excerpta Medica, 1978, pp 188–193

[31] Lawrence JH: Proton irradiation of the pituitary. Cancer 10:795–798, 1957

[32] Lawrence JH, Born JL, Tobias CA, et al: Clinical and metabolic studies in patients after alpha particle subtotal or total hypophysectomy. *In* Medicine in Japan in 1959. Proceedings of the 15th General Assembly of the Japan Medical Congress, Tokyo, 1959, pp 859–862

[33] Lawrence JH, Tobias CA, Born JL, et al: Heavy-particle irradiation in neoplastic and neurologic disease. J Neurosurg 19:717–722, 1962

[34] Levy RP, Fabrikant JI, Frankel KA, et al: Stereotactic heavy-charged-particle Bragg peak radiosurgery for the treatment of intracranial arteriovenous malformations in childhood and adolescence. Neurosurgery 24:841–852, 1989

[35] Levy RP, Fabrikant JI, Frankel KA, et al: Charged-particle radiosurgery of the brain. Neurosurg Clin North Am 1:955-990, 1990

[36] Levy RP, Fabrikant JI, Frankel KA, et al: Clinical-radiological evaluation of sequelae of stereotactic radiosurgery for intracranial arteriovenous malformations. (Lawrence Berkeley Laboratory Report LBL-28255, 1989.) *In* Proceedings of *Radiosurgery. A Neurosurgical Approach to Intracranial Lesions*, Charlottesville VA, 1990 (in press)

[37] Levy RP, Fabrikant JI, Phillips MH, et al: Stereotactic heavy-charged-particle Bragg peak radiosurgery for the treatment of intracranial angiographically-occult vascular malformations. (Lawrence Berkeley Laboratory Report LBL-28254, 1989.) *In* Proceedings of *Radiosurgery. A Neurosurgical Approach to Intracranial Lesions*, Charlottesville VA, 1990 (in press)

[38] Lo EH, Fabrikant JI, Levy RP, et al: A compartmental flow model for assessing response of intracranial AVMs to stereotactic radiosurgery. Neurosurgery 28:1251–1259, 1991

[39] Lo EH, Frankel KA, DeLaPaz RL, et al: Cerebrovascular and metabolic perturbations in delayed heavy charged particle radiation injury. Brain Res 504:168-172, 1989

[40] Lobato RD, Perez C, Rivas JJ, et al: Clinical, radiological, and pathological spectrum of angiographically occult intracranial vascular malformations J Neurosurg 68:518–531, 1988

[41] Ludewigt B, Chu W, Phillips M, et al: Accelerated helium-ion beams for radiotherapy and stereotactic radiosurgery. Med Phys (in press)

[42] Luessenhop AJ: Natural history of cerebral arteriovenous malformations. *In* Wilson CB, Stein BM (eds): Intracranial Arteriovenous Malformations, Baltimore, Williams & Wilkins, 1984, pp 12–23

[43] Lyman JT: Complication probability as assessed from dose-volume histograms. Radiat Res [Suppl] 104:S13-S19, 1985

[44] Lyman JT: Computer modeling of heavy charged-particle beams. *In* Skarsgard LD (ed): Pion and Heavy-ion Radiotherapy. Pre-clinical and Clinical Studies. New York, Elsevier Biomedical, 1983, pp 139–147

[45] Lyman JT, Chong CY: ISAH: A versatile treatment positioner for external radiation therapy. Cancer 34:12–16, 1974

[46] Lyman JT, Fabrikant JI, Frankel KA: Charged-particle stereotactic radiosurgery. Nucl Instrum Methods Phys Res B10/11:1107–1110, 1985

[47] Lyman JT, Frankel KA, Phillips MH, et al: Radiation physics for particle beam radiosurgery. Neurosurg Clin North Am (in press)

[48] Lyman JT, Howard J: Dosimetry and instrumentation for helium and heavy ions. Int J Radiat Oncol Biol Phys 3:81–85, 1977

[49] Lyman JT, Kanstein L, Yeater F, et al: A helium-ion beam for stereotactic radiosurgery of central nervous system disorders. Med Phys 13:695–699, 1986

[50] Lyman JT, Phillips MH, Frankel KA, et al: Stereotactic frame for neuroradiology and charged particle Bragg peak radiosurgery of intracranial disorders. Int J Radiat Oncol Biol Phys 16:1615–1621, 1989

[51] Marks MP, DeLaPaz RL, Fabrikant JI, et al: Intracranial vascular malformations: Imaging of charged particle radiosurgery. Part I. Results of therapy. Radiology 168:447–455, 1988

[52] Marks MP, DeLaPaz RL, Fabrikant JI, et al: Intracranial vascular malformations: Imaging of charged particle radiosurgery. Part II. Complications. Radiology 168:457–462, 1988

[53] Marks MP, Lane B, Steinberg GK, et al: Hemorrhage in intracerebral arteriovenous malformations: Angiographic determinants. Radiology 176:807–813, 1990

[54] Marks MP, O'Donahue J, Fabrikant JI, et al: Cerebral blood flow evaluation of arteriovenous malformations with stable xenon CT. AJNR 9:1169–1175, 1988

[55] Melnikov LA, Konnov BA, Yalynych NN: Radiosurgery of cerebral AVM. *In* Proceedings of the International Workshop on Proton and Narrow Photon Beam Therapy, Oulu, Finland, 1989, pp 92–98

[56] Minakova YeI: Review of twenty years proton therapy clinical experience in Moscow. *In* Proceedings of the Second International Charged Particle Workshop, Loma Linda, CA, 1987, pp 1–23

[57] Minakova YeI: Twenty years clinical experience of narrow proton beam therapy in Moscow. *In* Proceedings of the International Heavy Particle Therapy Workshop, Paul Scherrer Institute, Villigen, Switzerland, 1990, pp 158–162

[58] Minakova YeI, Krymsky VA, Luchin YeI, et al: Proton beam therapy in neurosurgical clinical practice (in Russian). Med Radiol (Mosk) 32:36–42, 1987

[59] Moses LE, Emerson JD, Hosseini H: Analyzing data from ordered categories. N Engl J Med 311:442-448, 1984

[60] Phillips MH, Frankel KA, Lyman JT, et al: Heavy-charged particle stereotactic radiosurgery: Cerebral angiography and CT in the treatment of intracranial vascular malformations. Int J Radiat Oncol Biol Phys 17:419–426, 1989

[61] Phillips MH, Frankel KA, Lyman JT, et al: Comparison of different radiation types and irradiation geometries in stereotactic radiosurgery. Int J Radiat Oncol Biol Phys 18:211–220, 1990

[62] Phillips MH, Kessler M, Frankel KA, et al: Image correlation of MRI, CT and cerebral angiography in the treatment planning for radiosurgery of intracranial arteriovenous malformations. Int J Radiat Oncol Biol Phys, 1990 (in press)

[63] Rodriguez A, Levy RP, Fabrikant JI: Experimental central nervous system injury after charged-particle irradiation. *In* Gutin PH, Leibel SA, Sheline GE (eds): Radiation Injury to the Nervous System. New York, Raven Press, 1991, pp 149–182

[64] Spetzler RF, Martin NA: A proposed grading system for arteriovenous malformations. J Neurosurg 65:476–483, 1986

[65] Spetzler RF, Selman WR: Pathophysiology of cerebral ischemia accompanying arteriovenous malformations. *In* Wilson CB, Stein BM (eds): Intracranial Arteriovenous Malformations. Baltimore, Williams & Wilkins, 1984, pp 24–31

[66] Stein BM: Surgical decisions in vascular malformations of the brain. *In* Barnett HJM, Stein BM, Mohr JP, Yatsu FM (eds): Stroke: Pathophysiology, Diagnosis, and Management, vol 2. New York, Churchill-Livingstone, 1986, pp 1129–1172

[67] Steinberg GK, Fabrikant JI, Marks MP, et al: Stereotactic heavy-charged-particle Bragg-peak radiation for intracranial arteriovenous malformations. N Engl J Med 323:96–101, 1990

[68] Steinberg GK, Levy RP, Fabrikant JI, et al: Stereotactic helium-ion Bragg peak radiosurgery for angiographically occult vascular malformations. *Harvard Radiosurgery Update*, Harvard Medical School, Chestnut Hill, MA, 1990 (abstract)

[69] Steiner L: Radiosurgery in cerebral arteriovenous malformations. *In* Fein JM, Flamm ES (eds): Cerebrovascular Surgery, vol 4. New York, Springer-Verlag, 1985, pp 1161–1215

[70] Tobias CA, Anger HO, Lawrence JH: Radiologic use of high energy deuterons and alpha particles. Am J Roentgenol Radium Ther Nucl Med 67:1–27, 1952

[71] Tobias CA, Lawrence JH, Born JL, et al: Pituitary irradiation with high-energy proton beams: A preliminary report. Cancer Res 18:121–134, 1958

[72] Tobias CA, Roberts JE, Lawrence JH, et al: Irradiation hypophysectomy and related studies using 340-MeV protons and 190-MeV deuterons. *In* Proceedings of the International Conference on the Peaceful Uses of Atomic Energy, Geneva, 1955, pp 95–106

[73] Valk PE, Dillon WP: Diagnostic imaging of central nervous system radiation injury. *In* Gutin PH, Leibel SA, Sheline GE (eds): Radiation Injury to the Nervous System. New York, Raven Press, chapter 13 (in press)

[74] Verhey L, Goitein M: Problems of inhomogeneities in particle beam therapy. *In* Skarsgard LD (ed): Pion and Heavy-ion Radiotherapy. Pre-clinical and Clinical Studies. New York, Elsevier Biomedical, 1983, pp 159–168

FIGURE LEGENDS

Figure 1: The Bragg ionization curve and its transverse profile for a typical 165-MeV/u helium-ion beam at the Bevatron at the University of California at Berkeley, Lawrence Berkeley Laboratory, modified for stereotactic radiosurgery of an intracranial AVM. **Left,** the peak-to-plateau ratio is approximately 3, and the relative biologic effectiveness in the peak is estimated to be about 1.3; thus the biologic effect in the peak is about 4 times that of the plateau region. The dose fall-off in the distal peak from 90% to 10% is about 2-3 mm. **Right,** the transverse profile of the peak demonstates sharp lateral edges, and the dose fall-off from 90% to 10% is about 2.5 mm. This profile was measured 1 cm proximal to the distal edge of a beam with a 7-cm residual range and with the Bragg peak spread 2 cm. The distal edge of the Bragg peak and the lateral sharpness are negligibly affected by spreading the Bragg peak.

Figure 2: The charged-particle beam delivery system for stereotactic radiosurgery of intracranial tumors and vascular disorders at the University of California at Berkeley, Lawrence Berkeley Laboratory 184-inch synchrocyclotron. The stereotactic patient positioning system (ISAH) permits translation along 3 orthogonal axes (x,y,z) and rotation about the y and z axes and provides precise patient immobilization and positioning at the isocenter for stereotactically directed charged-particle-beam therapy. The width of the high-dose Bragg ionization peak within the brain can be spread to the prescribed size by interposing a modulating filter of comparable maximum thickness (x cm) in the beam path. At the Bevatron accelerator, the Bragg ionization peak is modulated by use of a computer-controlled variable-position water column absorber. The range in tissue of the Bragg peak region is determined by a range-modifying absorber. An individually designed aperture, specifically tailored to the size and configuration of the lesion, shapes each beam in cross section. Tissue-equivalent compensators adjust for skull curvature and tissue inhomogeneities and further improve the precision placement of the Bragg peak region. The ion chamber monitors the dose delivered by each beam. Multiple entry angles and beam ports

are chosen with appropriate modification of radiation parameters, so that the high-dose regions of the individual beams intersect and stop within the defined target and the lowest possible dose reaches sensitive adjacent normal brain tissues. (*From* Levy RP, Fabrikant JI, Frankel KA, Phillips MH, Lyman JT: Stereotactic heavy-charged-particle Bragg peak radiosurgery for the treatment of intracranial arteriovenous malformations in childhood and adolescence. Neurosurgery 24:842, 1989; with permission.)

Figure 3: Stereotactic frame and patient mask system (cf Fig. 4). The head immobilization mask is formed of thermoplastic material and molded to each patient's head. Letters denote components of the stereotactic frame: (A) Top cross member. (B) Yoke. (C) Graphite support bar. An identical bar is present on the other side of the frame. A fiducial marker is present on each bar. (D) Sideplates with fiducial markers. The clear lucite sideplates have two grooves machined at right angles. Fine copper wires glued into the grooves serve as markers for angiograms and CT and are imaged on lateral radiographs. For MRI, fine tubes filled with olive oil are substituted into the grooves. (E) Arch with fiducial markers. Arch supports two copper wire markers (or oil-tube markers for MRI) that are imaged on anteroposterior radiographs. (F) Positioning pins. The mask is reliably positioned by means of carefully placed holes that correspond to the three pins. (*From* Lyman JT, Phillips MH, Frankel KA, Fabrikant JI: Stereotactic frame for neuroradiology and charged particle Bragg peak radiosurgery of intracranial disorders. Int J Radiat Oncol Biol Phys 16:1617, 1989; with permission.)

Figure 4: Schematic of the stereotactic frame for neuroradiologic imaging and radiosurgery (cf Fig. 3). The components of the frame are illustrated, and the relationships between the fiducial markers and structural components are shown. (*From* Lyman JT, Phillips MH, Frankel KA, Fabrikant JI: Stereotactic frame for neuroradiology and charged particle Bragg peak radiosurgery of intracranial disorders. Int J Radiat Oncol Biol Phys 16:1617, 1989; with permission.)

Figure 5: The anatomic and neuroradiologic basis for treatment planning of stereotactic

heavy charged-particle Bragg peak radiosurgery for intracranial vascular disorders integrates information from the stereotactic cerebral angiogram (left), CT scans (**upper right and middle right**), and MRI scans (**lower right**). The data are used for target contouring and conversion to relative stopping-power values for optimal dose distribution and dose localization. (*From* Fabrikant JI, Frankel KA, Phillips MH, Levy RP: Stereotactic heavy charged-particle Bragg peak radiosurgery for intracranial arteriovenous malformations. *In* Edwards MSB, Hoffman HJ (eds): Cerebral Vascular Disease in Children and Adolescents, Baltimore, Williams & Wilkins, 1989, p 392; with permission.)

Figure 6: The helium-ion beam path is shown in relation to the stereotactically determined isocenter of the patient positioning system, the Irradiation Stereotactic Apparatus for Humans (ISAH) in the medical cave of the 184-inch synchrocyclotron at the University of California at Berkeley, Lawrence Berkeley Laboratory. The immobilization system is used for both Bragg peak and plateau-region heavy charged-particle radiosurgery for arteriovenous malformations, pituitary tumors, and other intracranial targets. (*From* Fabrikant JI, Lyman JT, Frankel KA: Heavy charged-particle Bragg peak radiosurgery for intracranial vascular disorders. Radiat Res [Suppl] 104:S247, 1985; with permission.)

Figure 7: Computer-reformatted overlay of digitized angiographic films for treatment-planning procedures, used to transfer the three-dimensional target volume for dose localization and to align the patient for the radiosurgical procedure. The overlay contains the fiducial markers, the target contours, midplane cranial bony landmarks, and the position of the isocenter of the patient positioner (denoted by the cross). **Upper**, lateral and anteroposterior views demonstrate relative orientation of these elements when the stereotactic frame center is located at the ISAH isocenter; note perfect alignment of fiducial markers on lateral view (**upper left**). **Lower**, corresponding views demonstrate relative orientation when the patient has been moved so as to place the center of the lesion at the isocenter of the immobilization system ("treatment position"). The two concentric target contours (**lower**) are the target contour magnified to match the port-film localization radiograph

during treatment (outer contour), and the actual size of the AVM (inner contour). (*From* Phillips MH, Frankel KA, Lyman JT, Fabrikant JI, Levy RP: Heavy charged-particle stereotactic radiosurgery: Cerebral angiography and CT in the treatment of intracranial vascular malformations. Int J Radiat Oncol Biol Phys 17:423, 1989; with permission.)

Figure 8: Stereotactic heavy charged-particle Bragg peak radiosurgery treatment plan (helium ions, 230 MeV/u) for a patient with a brain-stem AVM (the inner ring of white dots represents the angiographically defined lesion, to which the 90% isodose surface is contoured). The unmodified helium-ion beam was collimated by an 8-mm circular brass aperture. Treatment was performed using four coplanar ports in 1 day to a volume of 0.25 cm^3 (dose, 45 GyE). (*From* Fabrikant JI, Lyman JT, Frankel KA: Heavy charged-particle Bragg peak radiosurgery for intracranial vascular disorders. Radiat Res [Suppl] 104:S246, 1985; with permission.)

Figure 9: Stereotactic helium-ion Bragg peak radiosurgery treatment plan for a large left temporal and deep central nuclei AVM in a 39-year-old man (angiograms of the AVM are shown in Fig. 10). **Left**, axial plane; **right**, sagittal plane. The helium-ion beam was collimated by 61 x 50 mm and 55 x 42 mm individually shaped brass and cerrobend apertures; 27 GyE was delivered in 3 days to the lesion (defined by the ring of white dots; volume, 54 cm^3) using four noncoplanar beams through multi-angled ports. The 90% isodose contour borders precisely on the periphery of the lesion. There is rapid dose fall-off to the 70% level, and the 10% isodose contour completely spares irradiation of the contralateral hemisphere. The treatment plan illustrates the unique physical advantages of stereotactic radiosurgery with charged-particle beams, especially for large and irregularly shaped AVMs.

Figure 10: Stereotactic cerebral angiograms in a 39-year-old man with a large (54 cm^3) left hemispheric AVM (cf Fig. 9). **Upper**, lateral left internal carotid artery (**left**) and vertebral artery (**right**) angiograms demonstrate the size, shape, and location of the AVM which is supplied by branches of the left middle cerebral and vertebral arteries. The

vascular steal is pronounced, and the entire ipsilateral cortex is underperfused. **Lower,** lateral left carotid artery **(left)** and vertebral artery **(right)** angiograms taken 12 months after radiosurgery (dose, 27 GyE) demonstrate complete obliteration of the malformation. The vascular steal has been reversed, and normal or near-normal hemodynamic conditions have been restored. The patient demonstrated transiently symptomatic moderate vasogenic edema in the deep white matter of the irradiated hemisphere. This edema subsequently resolved spontaneously.

Figure 11: Stereotactic heavy charged-particle Bragg peak radiosurgery treatment plan for a 29-year-old woman with a symptomatic angiographically occult vascular malformation in the pons. **Left (upper and lower),** diagnostic stereotactic MRI images (with the patient in the immobilizing mask and stereotactic frame) in the axial and sagittal planes are used to define the target volume (ring of white dots) for stereotactic radiosurgery. The target contour data then are transferred to corresponding stereotactic CT images, using correlative MRI and CT procedures and software for the VAX 11/780 computer system. **Middle (upper and lower),** CT data then are used to identify and compensate for inhomogeneities in the tissues to be traversed by the charged-particle beams and to calculate three-dimensional dose-distribution contours. **Right (upper and lower),** the isodose contour information then is transferred back to the original MR images to permit the explicit demonstration (and modification, where required) of isodose contour distributions in all desired anatomic planes. Isodose contours displayed here in the axial and sagittal planes are calculated for 10, 50, 70, and 90% of the maximum central dose.

Figure 12: Sagittal MR image in a 35-year-old man with a pontine angiographically occult vascular malformation shows the isodose contours for multi-angle stereotactic helium-ion Bragg peak radiosurgery. The malformation initially was defined and contoured on stereotactic MRI scans and this data was transferred to stereotactic CT images; the treatment plan was calculated using the CT data. The resulting isodose contours then were transferred back to the original sagittal MR images, to determine the radiation dose to the

target volume and adjacent brain-stem structures. The treatment plan is a composite for three helium-ion beams; one port is in the sagittal plane (shown); the other two ports are in parasagittal planes at ±30 degrees, to direct the multi-angle beams parallel to the bony structures of the petrous pyramids. (*From* Levy RP, Fabrikant JI, Frankel KA, Phillips MH, Lyman JT: Charged-particle radiosurgery of the brain. Neurosurg Clin North Am 1:983, 1990; with permission.)

Figure 13: Cerebral angiograms in a 10-year-old boy with a history of subarachnoid hemorrhage from a large (26 cm^3) right frontotemporal AVM. **Upper**, lateral and antero-posterior views of the right internal carotid artery angiogram demonstrate the size, shape, and location of the AVM, which is supplied by branches of the right middle and anterior cerebral arteries. Surgical excision was attempted, but extreme vascular friability and consequent blood loss during surgery required that the procedure be terminated before any resection could be accomplished. The patient then was treated with heavy-charged-particle Bragg peak radiosurgery; a dose of 28 GyE helium ions (230 MeV/u) was delivered through five ports in 2 days. **Lower**, lateral and anteroposterior views from the angiogram performed 12 months after radiosurgery demonstrate complete obliteration of the malformation. The patient remained normal 66 months after treatment. (*From* Fabrikant JI, Frankel KA, Phillips MH, Levy RP: Stereotactic heavy-charged-particle Bragg peak radiosurgery for intracranial arteriovenous malformations. *In* Edwards MSB, Hoffman HJ (eds): Cerebral Vascular Disease in Children and Adolescents. Baltimore, Williams & Wilkens, 1989, p 404; with permission.)

Figure 14: Cerebral angiograms in a 23-year-old man with a history of refractory seizures from a large (40 cm^3) left frontotemporal AVM. **Upper**, lateral and anteroposterior views of the internal carotid artery angiogram demonstrate the AVM supplied by branches of the anterior and middle cerebral artery circulations. The vascular steal is prominent. **Lower**, comparable views taken 18 months after helium-ion radiosurgery (dose, 28 GyE) demonstrate complete obliteration of the AVM. Normal cerebral blood flow has been re-

stored, with marked reversal of the vascular steal. (*From* Levy RP, Fabrikant JI, Frankel KA, Phillips MH, Lyman JT: Charged-particle radiosurgery of the brain. Neurosurg Clin North Am 1:980, 1990; with permission.)

Figure 15: Kaplan-Meier cumulative plots for the temporal distribution of complete AVM obliteration as a function of the volume of the AVM prior to helium-ion radiosurgery in 71 patients who had angiographic follow-up. Solid line, pretreatment angiographic volumes <4 cm^3 (23 patients); dashed line, volumes 4 cm^3 to 25 cm^3 (28 patients); dotted line, volumes >25 cm^3 (20 patients). Vertical lines represent patients with residual malformations. Smaller lesions obliterate most frequently and with the shortest latency intervals. (*From* Steinberg GK, Fabrikant JI, Marks MP, Levy RP, Frankel KA, Phillips MH, Shuer LM, Silverberg GD: Stereotactic heavy-charged-particle Bragg-peak radiation for intracranial arteriovenous malformations. N Engl J Med 323:99, 1990; with permission.)

Figure 16: Stereotactic cerebral angiograms in an 18-year-old woman with a deep right parietal AVM. **Left (upper and lower)**, lateral and anteroposterior views demonstrate the AVM prior to stereotactic helium-ion radiosurgery (treatment volume, 3.4 cm^3). **Middle (upper and lower)**, 12 months after radiosurgery (dose, 20 GyE) there was partial obliteration of the AVM. **Right (upper and lower)**, 24 months after radiosurgery the AVM was completely obliterated. The patient remained neurologically normal throughout this period despite developing vasogenic edema (cf Fig. 17).

Figure 17: Sequential T2-weighted MRI, same patient whose cerebral angiograms are shown in Figure 16. **Left (upper)**, before stereotactic radiosurgery. **Right (upper)**, little change had occurred 8 months after treatment. **Left (lower)**, vasogenic edema had spread into the the deep white matter of the parietal lobe 16 months after treatment. **Right (lower)**, the edema had resolved 22 months after treatment. The patient was asymptomatic throughout this course and required no corticosteroid therapy.

Figure 18: Sequential axial MR images in a 15-year-old girl with a large (25 cm^3) left parietal AVM. A dose of 32 GyE was delivered to the AVM using four ports in 2 days.

Progressive vasogenic edema and mild right-sided hemiparesis subsequently developed but improved markedly with corticosteroid therapy. Currently, she has only minimal intermittent neurologic impairment, an *excellent* clinical grade, and no longer requires steroids. Her AVM has been fully obliterated (see text). **Upper (left)**, MRI before stereotactic heavy-charged-particle Bragg peak radiosurgery; **(middle)**, 13 months after treatment, initial MRI signs of deep white-matter edema were seen; **(right)**, 20 months after treatment, mass effect was demonstrated, at which time the initial signs of mild hemiparesis became clinically apparent, and she began receiving steroids. **Lower (left)**, 24 months after treatment, the edema began to resolve and there was marked clinical improvement with steroid therapy; **(middle)**, 30 months after treatment, with further resolution of edema, steroids were discontinued; **(right)**, 34 months after treatment, only subtle neurologic dysfunction remained. The AVM was completely obliterated, and the most recent MRI demonstrated progressive resolution of the vasogenic edema. (*From* Levy RP, Fabrikant JI, Frankel KA, Phillips MH, Lyman JT: Stereotactic heavy-charged-particle Bragg peak radiosurgery for the treatment of intracranial arteriovenous malformations in childhood and adolescence. Neurosurgery 24:849, 1989; with permission.)

Figure 19: **Upper (left and right)**, lateral and anteroposterior angiograms of the right internal carotid artery in a 33-year-old man before radiosurgery for a large (18 cm^3) deep right parietal AVM. **Middle (left and right)**, comparable views, 12 months after treatment with 30 GyE, demonstrate partial obliteration of the AVM. **Lower (left and right)**, coronal and axial MR images 21 months after treatment show extensive abnormal high-intensity signal in the right parietal lobe, associated with development of left-sided hemiparesis; angiography at this time demonstrated complete obliteration of the AVM. The patient's left-sided weakness improved markedly with corticosteroid therapy but recurred when steroids were tapered. An exploratory craniotomy 33 months after treatment revealed underlying radiation necrosis.

Figure 20: A large left frontoparietal AVM in a 35-year-old man, 24 months following

heavy-charged-particle radiosurgery (helium ions; dose, 35 GyE). **Left**, marked depression of glucose metabolism in the deep white matter of the left parietal cortex is demonstrated on an [18]fluorodeoxyglucose positron-emission tomographic image (taken with the Donner Laboratory 600 crystal detector high-resolution PET scanner). **Right**, the corresponding MR image shows intense signal in the deep white matter in the same region; the changes are associated with profound vasogenic edema. The patient was clinically normal at this time, but 18 months later, mild right-sided hemiparesis developed along with clumsiness of hand and foot function and diminished mentation. Gadolinium-enhanced MRI suggested an underlying focus of radiation necrosis, and surgical exploration found a well-defined region of necrosis. The AVM was thrombosed, and part of the thrombosed vascular mass and necrotic tissue were removed. The patient subsequently showed significantly improved clinical status, returned to work, and regained an *excellent* clinical grade. (*From* Valk PE, Dillon WP: Diagnostic imaging of central nervous system radiation injury. *In* Gutin PH, Leibel SA, Sheline GE (eds): Radiation Injury to the Nervous System. New York, Raven Press, 1990, in press; with permission.)

Figure 21: Deep left parietal AVM in a 15-year-old boy, residual after partial surgical excision. **Upper** (**left and middle**), stereotactic lateral and anteroposterior angiograms of the left internal carotid artery and (**right**) contrast-enhanced CT demonstrate the AVM prior to radiosurgery. **Lower**, comparable views on angiograms (**left, middle**) and CT (**right**) 12 months after treatment with 25 GyE demonstrate complete obliteration of the AVM without evidence of edema. Moderate right-sided hemiparesis that was unresponsive to steroids began shortly before the 12-month follow-up studies were performed; small vessel occlusion was presumed to be responsible for this deficit. This patient has had an incomplete recovery, and his clinical grade is *good*.

Figure 22: Images from sequential radiographic studies in a 40-year-old woman with a history of disabling headaches and intracranial hemorrhage from a very large (40 cm^3) right temporal AVM. A dose of 28 GyE was delivered to the AVM using five ports in 2 days.

Upper (left), stereotactic cerebral angiogram, anteroposterior view, of the right vertebral artery prior to stereotactic heavy charged-particle Bragg peak radiosurgery; **(middle)**, T2-weighted axial MRI obtained at 23 months after treatment demonstrates vasogenic edema pattern in the deep white matter; **(right)**, complete obliteration of the AVM is shown by angiography 27 months after treatment; the vascular patterns of the normal cerebral vessels are undisturbed and intact. **Lower (left)**, complete stenosis of the right posterior cerebral artery, associated with left-sided hemiparesis, is seen on vertebral artery angiograms performed 28 months after treatment; **(right)**, T2-weighted axial MRI at 28 months shows high-intensity signal, consistent with cerebral infarction, in gray and deep white matter. Currently, the patient's neurologic deficit is stable, and her clinical grade is *good. (From* Marks MP, DeLaPaz RL, Fabrikant JI, Frankel KA, Phillips MH, Levy RP, Enzmann DR: Imaging of charged-particle stereotactic radiosurgery for intracranial vascular malformations. Part II. Complications. Radiology 168:462, 1988; with permission.)

Figure 23: Large (24 cm^3) high-flow left posterior parietal AVM in a 32-year-old woman, before radiosurgery. Left internal carotid artery angiograms **(upper)** in lateral **(left)** and anteroposterior **(right)** views and vertebral artery angiograms **(lower)** in lateral **(left)** and anteroposterior **(right)** views demonstrate the AVM, which is supplied by branches of the left middle and left posterior cerebral arteries. The vascular steal is pronounced. The patient was treated with helium-ion radiosurgery; a dose of 25 GyE was delivered through seven ports in 2 days. (Cf Fig. 24.)

Figure 24: Ten months after treatment for the AVM in Figure 23, the patient sustained a subarachnoid hemorrhage from a ruptured aneurysm of the basilar artery tip, demonstrated by lateral and anteroposterior views of the vertebral artery angiogram **(left, upper and lower)**. This aneurysm (arrows) had not been demonstrated by angiographic studies prior to radiosurgery (cf Fig. 23). The treatment had induced a near-complete obliteration of the AVM at the time of aneurysm hemorrhage. It appears that, as the cerebrovascular blood flow was normalizing during the process of obliteration of the high-volume, high-flow

AVM, the resulting increase in the regional cerebral vascular resistance was transmitted to the vertebral artery branches, and that this hemodynamic change was sufficient to induce expansion of the previously dormant aneurysm, leading to hemorrhage. The aneurysm was surgically clipped. A few months later, left internal carotid artery angiograms in lateral and anteroposterior views (**Upper, middle and right**), and vertebral artery angiograms in lateral and anteroposterior views (**lower, middle and right**) demonstrated complete obliteration of the large AVM (cf Fig. 23). The vascular steal has been reversed, and the patient has recovered fully.

Figure 25: The frequency of clinical complications (major and minor) following heavy charged-particle radiosurgery in relation to treatment dose and volume of treated AVM in 86 patients. The physical doses (ordinate) and *angiographic* volumes (abscissa) are given. (The biologically equivalent dose is calculated based on a relative biologic effectiveness of 1.3 for the Bragg ionization peak.) Open circles, patients with complications; solid circles, patients with no complications. (*From* Steinberg GK, Fabrikant JI, Marks MP, Levy RP, Frankel KA, Phillips MH, Shuer LM, Silverberg GD: Stereotactic heavy-charged-particle Bragg-peak radiation for intracranial arteriovenous malformations. N Engl J Med 323:100, 1990; with permission.)

Figure 26: Stereotactic cerebral angiograms of a large, deep, right parietal AVM in a 32-year-old man. **Upper (left and right)**, lateral and anteroposterior views of the right internal carotid artery demonstrate the AVM prior to radiosurgery. A rectangular "target" (marked in orthogonal projections), assumed to be the AVM "nidus," was designated as the radiosurgical target volume; the volume treated was 7 cm^3. **Lower (left and right)**, comparable angiographic views 34 months after radiosurgery (dose, 35 GyE). There has been almost complete obliteration of the abnormal shunting vessels in the irradiated target volume but no change in the unirradiated peripheral shunts of the AVM.

Figure 27: Positron-emission tomography performed on the Donner Laboratory PET unit demonstrates progressive physiologic changes in the brain of a 37-year-old woman whose

large (14 cm^3) right hemispheric AVM, located in the deep white matter, was treated with helium-ion radiosurgery (dose, 32 GyE). **Upper**, 21 months after radiosurgery, when she experienced progressive left-sided hemiparesis; MRI at that time demonstrated extensive vasogenic edema in the right hemisphere; **left**, ^{82}Rb PET scan shows a focal region of blood-brain barrier (BBB) disruption in the irradiated right hemisphere; no BBB disruption is seen in the unirradiated contalateral hemisphere; **middle**, the corresponding ^{18}FDG PET image shows decrease in the tracer uptake, indicating metabolic depression throughout the irradiated hemisphere; there is high metabolic activity in the unirradiated thalamus; **right**, ^{122}I-HIPDM tracer reveals decreased blood flow in the right cortex and in the region of the AVM, with increased tracer activity and blood flow in the unirradiated cortex. **Lower**, by 33 months, she had developed dense hemiparesis on the left side; the MRI studies demonstrated profound vasogenic edema limited to the left hemisphere; **left**, the ^{82}Rb PET tracer study reveals persistent disruption of the BBB; **middle**, ^{18}FDG tracer studies indicate worsening of the metabolic depression throughout the irradiated hemisphere; high metabolic activity persists in the unirradiated thalamus and cortex. (In collaboration with P. E. Valk).

Figure 28: The xenon-enhanced CT image in a patient with a left parietal-occipital AVM demonstrates significant regional cerebral blood flow (rCBF) "steal" phenomenon in the entire ipsilateral cortex and diminished flow in regions of the contralateral cortex. The cerebral map is quantified in relation to defined rCBF and is used clinically to assess the process of cerebral blood flow normalization after radiosurgery. (*From* Fabrikant JI, Frankel KA, Phillips MH, Levy RP: Stereotactic heavy charged-particle Bragg peak radiosurgery for intracranial arteriovenous malformations. *In* Edwards MSB, Hoffman HJ (eds): Cerebral Vascular Disease in Children and Adolescents, Baltimore. Williams & Wilkins, 1989, p 406; with permission.)

TABLE 1. CHARACTERISTICS of HELIUM-ION BEAMS for RADIOSURGERY

	184-Inch Synchrocyclotron	Bevatron
Energy (MeV/u)	230	165
90% dose range (mm)	145	141
Peak-plateau ratio	3.1	5.5
90% peak width (mm)	5.2	1.6
80% peak width (mm)	7.8	2.7
50% peak width (mm)	40.0	9.0
Distal fall-off (%/mm)	14 ± 2.5	43 ± 6.7
Exit dose (%D_{max} *)	≈ 2.6	≈ 1.8

*D_{max} = maximum dose.

Adapted from Lyman JT, Fabrikant JI, Frankel KA: Charged-particle stereotactic radiosurgery. Nucl Instrum Methods Phys Res B10/11:1109, 1985.

TABLE 2. CLINICAL GRADE at LAST FOLLOW-UP in 101 PATIENTS*

Presenting	No. (%) of Patients Graded as			
Grade	Excellent	Good	Poor	Dead
Excellent				
68 (67%)	53 (78%)	12 (18%)	2 (3%)	1 (1%)
Good				
29 (29%)	5 (17%)	21 (72%)	2 (7%)	1 (3%)
Poor				
4 (4%)	0	1 (25%)	0	3 (75%)
All Grades				
101 (100%)	58 (57%)	34 (34%)	4 (4%)	5 (5%)

*Evaluated using Drake scale [7,8] before and after radiosurgical treatment in the UCB-SUMC series. Total includes 15 patients with AOVMs.

TABLE 3. COMPLETE AVM OBLITERATION vs VOLUME

| Volume (cm^3)* | No. (%) of Patients with Complete Obliteration at | | |
	1 year	2 years	3 years
<4	9/17 (53%)	17/18 (94%)	18/18 (100%)
4 - 25	7/24 (29%)	15/20 (75%)	19/20 (95%)
>25	1/18 (6%)	7/18 (39%)	7/10 (70%)
All	17/59 (29%)	39/56 (70%)	44/48 (92%)

*Angiographically determined volume before helium-ion radiosurgery
(see section on Neuroradiologic Evaluation).

TABLE 4. COMPLETE AVM OBLITERATION vs TREATMENT DOSE

Dose (GyE)*	No. (%) of Patients with Complete Obliteration at		
	1 year	2 years	3 years
11.5-20	3/18 (17%)	6/12 (50%)	6/6 (100%)
24-28	5/25 (20%)	17/26 (65%)	19/22 (86%)
30-45	9/16 (56%)	16/18 (89%)	19/20 (95%)

*Physical dose in Gy multiplied by a relative biologic effectiveness of 1.3
for the Bragg ionization peak of helium ions.

Adapted from Steinberg GK, Fabrikant JI, Marks MP, Levy RP, Frankel KA,
Phillips MH, Shuer LM, Silverberg GD: Stereotactic heavy-charged-
particle Bragg-peak radiation for intracranial arteriovenous malformations.
N Engl J Med 323:99, 1990.

TABLE 5. CHARGED-PARTICLE RADIOSURGERY for INTRACRANIAL VASCULAR DISORDERS

Clinical Condition	Number of Patients			
	UCB-LBL[a] (1980-Oct.1990)	HCL-MGH[b] (1965-Oct.1989)	BNI-ITEP[c] (1983-Oct.1990)	LINPh[d] (1978-Feb.1990)
Arteriovenous malformation (angiographically demonstrable)	346	1209	66	187
Occult vascular malformation	42	98	-	-
Cavernous-carotid fistula	2	-	24	-
Arterial aneurysm	-	-	-	6
Total	390	1307	90	193

[a] UCB-LBL: University of California at Berkeley - Lawrence Berkeley Laboratory
[b] HCL-MGH: Harvard Cyclotron Laboratory - Massachussetts General Hospital (personal communication, R. N. Kjellberg - Oct. 1989)
[c] BNI-ITEP: Burdenko Neurosurgical Institute - Institute for Theoretical and Experimental Physics (personal communication, Ye. I. Minakova - Oct. 1990)
[d] LINPh: Leningrad Institute of Nuclear Physics (personal communication, B. A. Konnov - Feb. 1990)
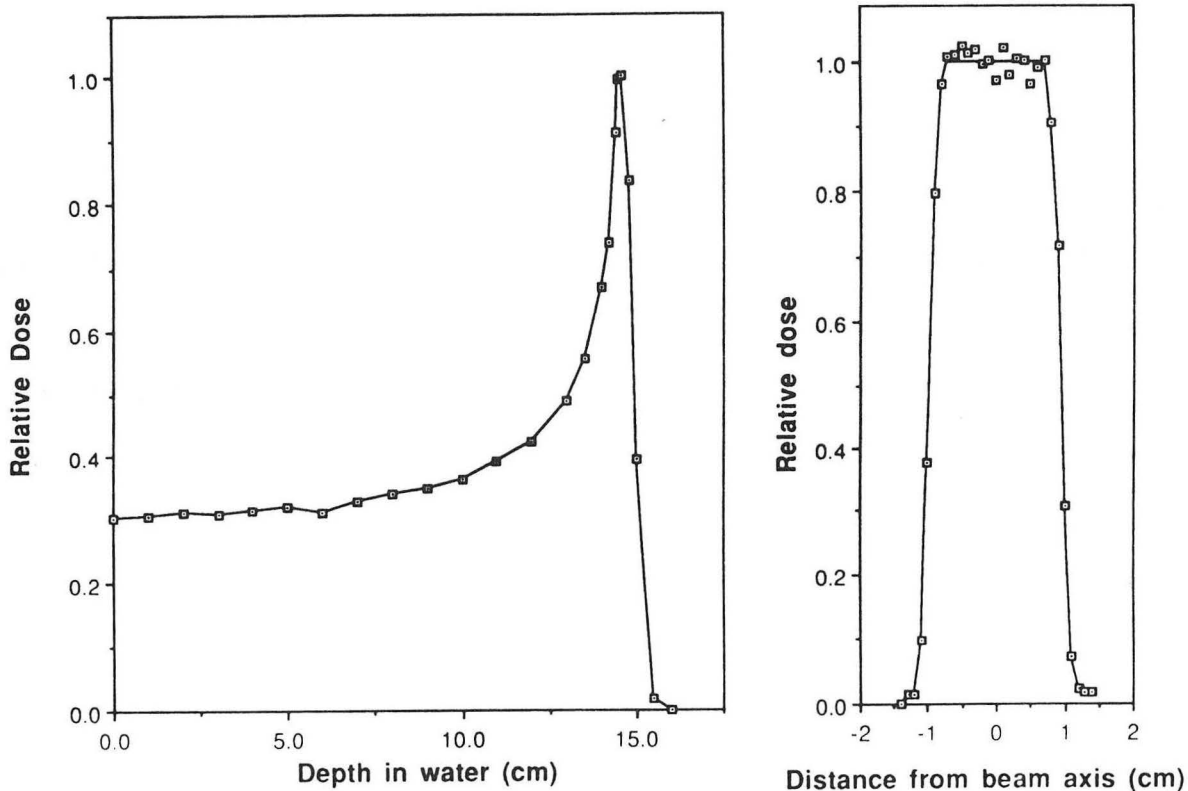
Figure 1

XBL 9012-3874

Charged Particle Beam Delivery System
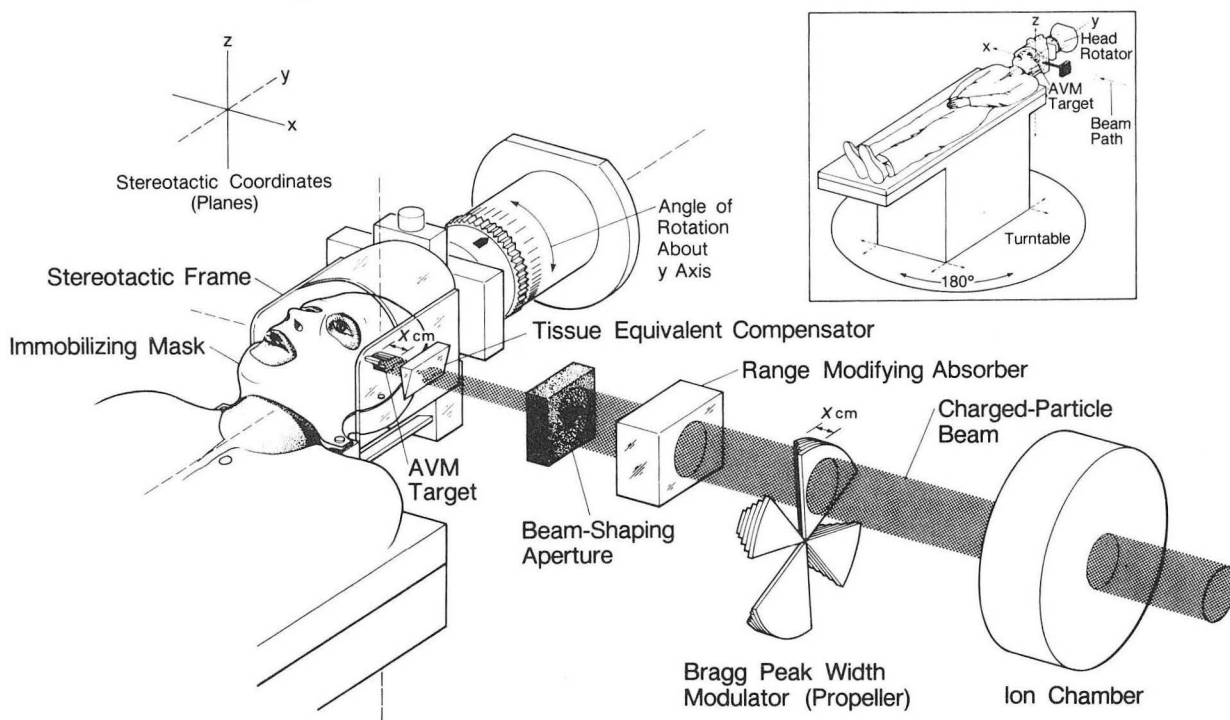
Figure 2

XBL 8810-7674

Figure 3

CBB 877-5479

Anterior Fiducial
Markers

Arch

Mask
Positioning Pin

Sideplate

Yoke

Top
Cross-member

Posterior Fiducial
Markers

Lateral Fiducial
Markers

Support Rod

XBL 889-7575

Figure 4

STEREOTACTIC RADIOSURGERY

Arteriovenous malformation

Mid line

Computerized Tomograph

Isodose Contours

CBB 843-1469

Magnetic Resonance Image

Isodose Contours

Figure 5

I.S.A.H.

Range modulator

Ion chamber

Iron collimator

Degrader

Patient collimator

Beam path

Head rotator

Brass collimator

Turntable

Figure 6

XBL 824-486

Figure 7

XBB 853-1740

Figure 8
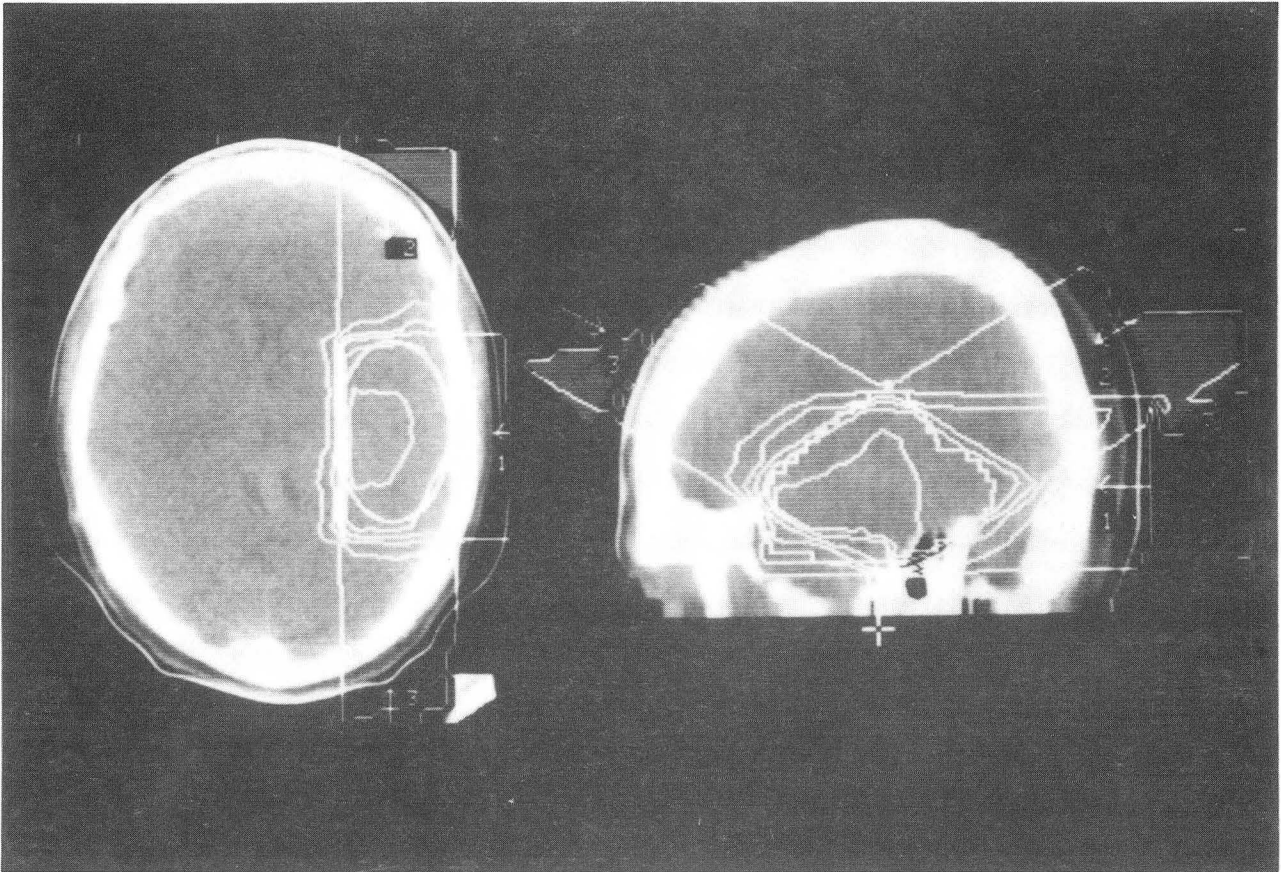
Figure 9
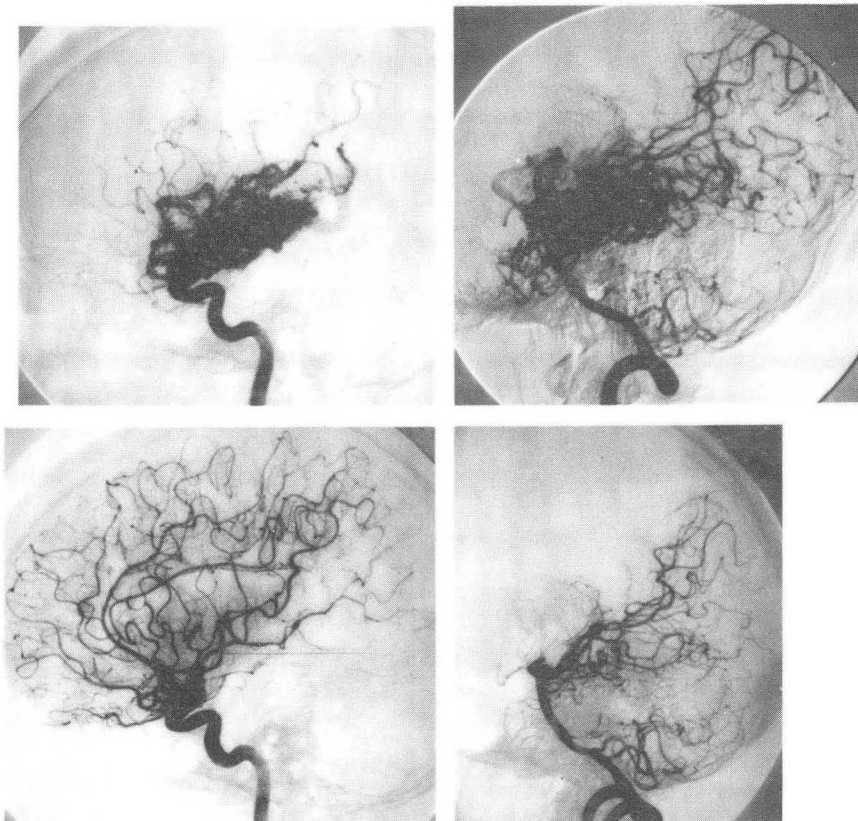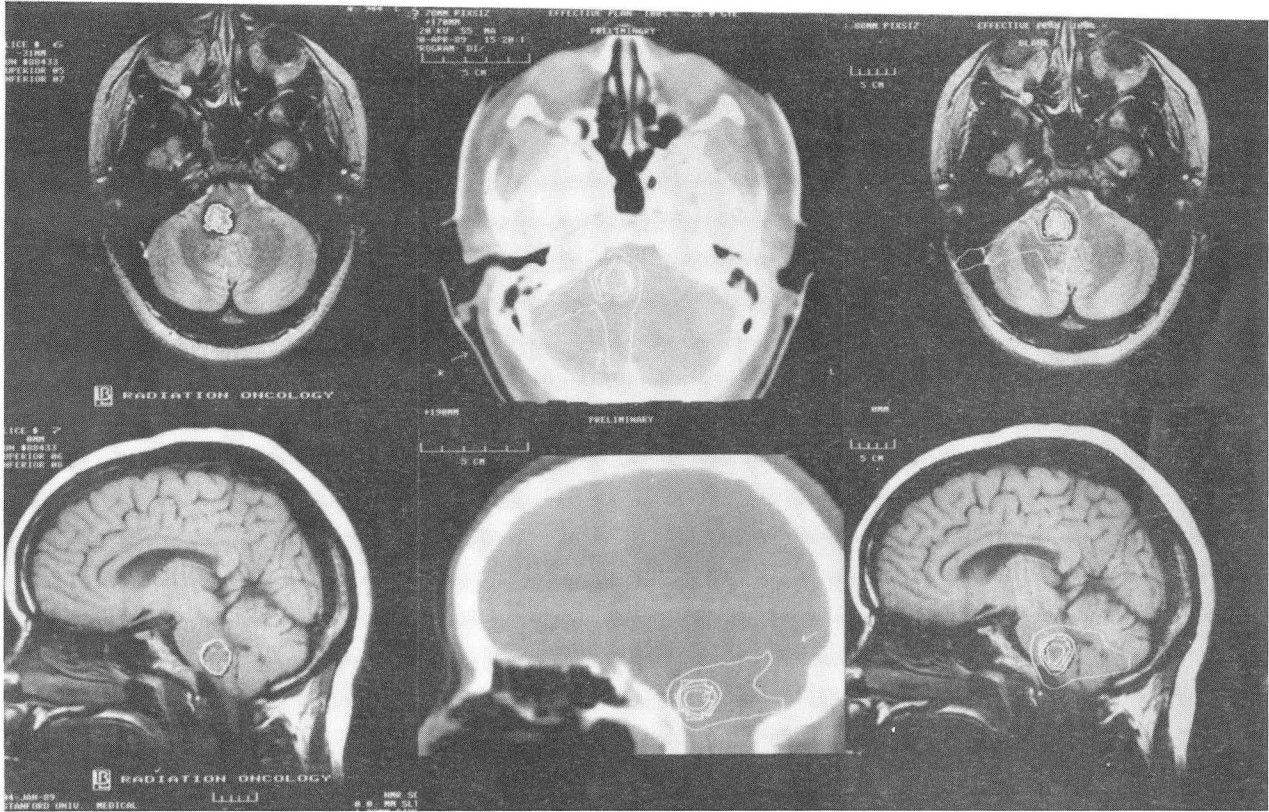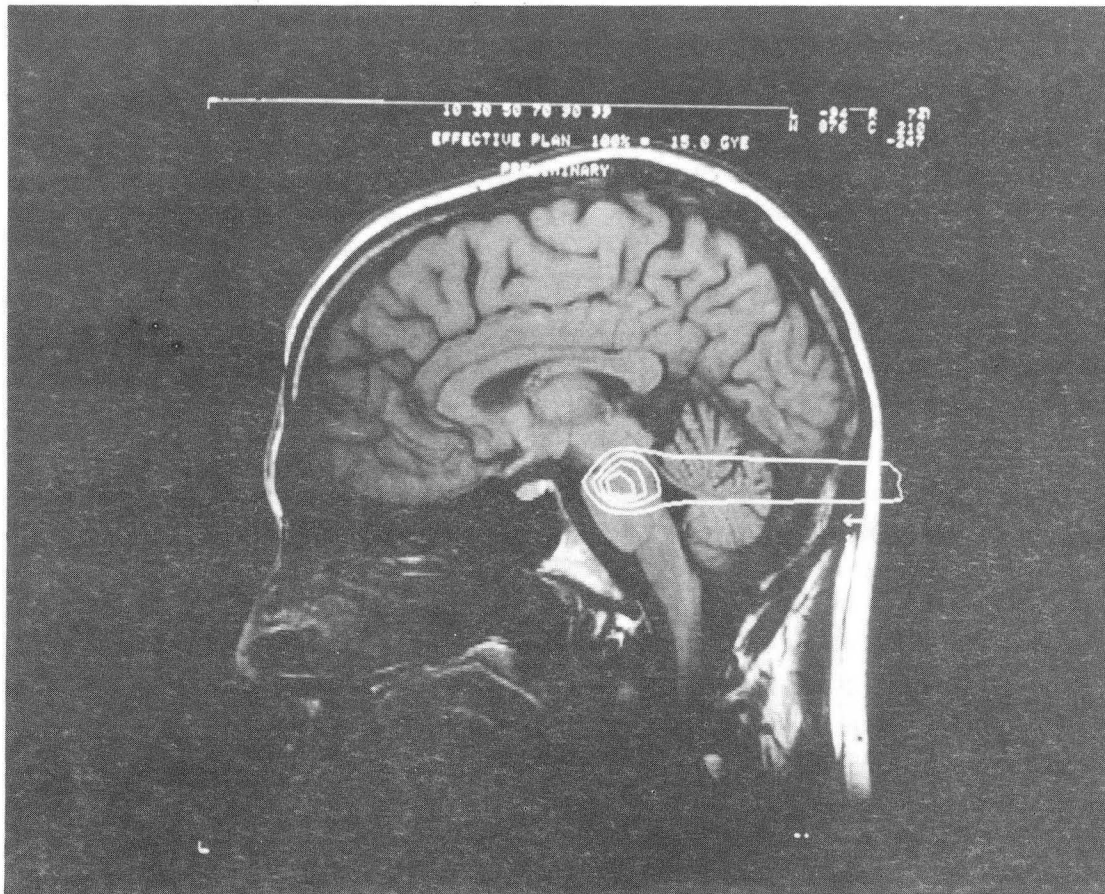
Figure 10
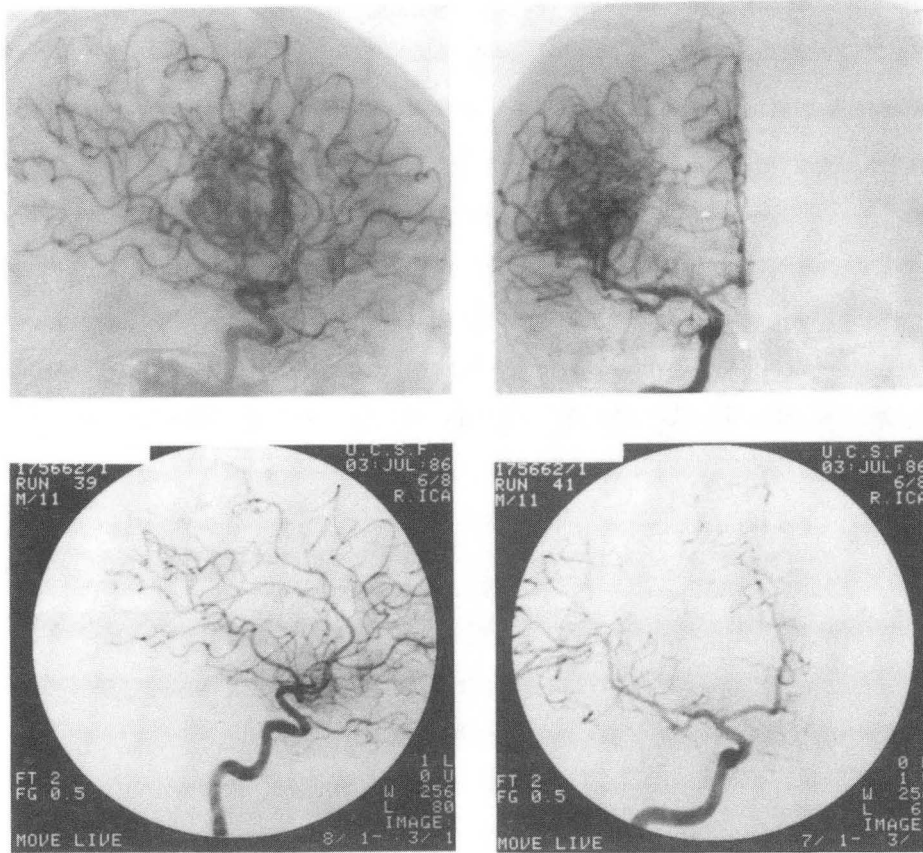
Figure 11

Figure 12

XBB 871-79
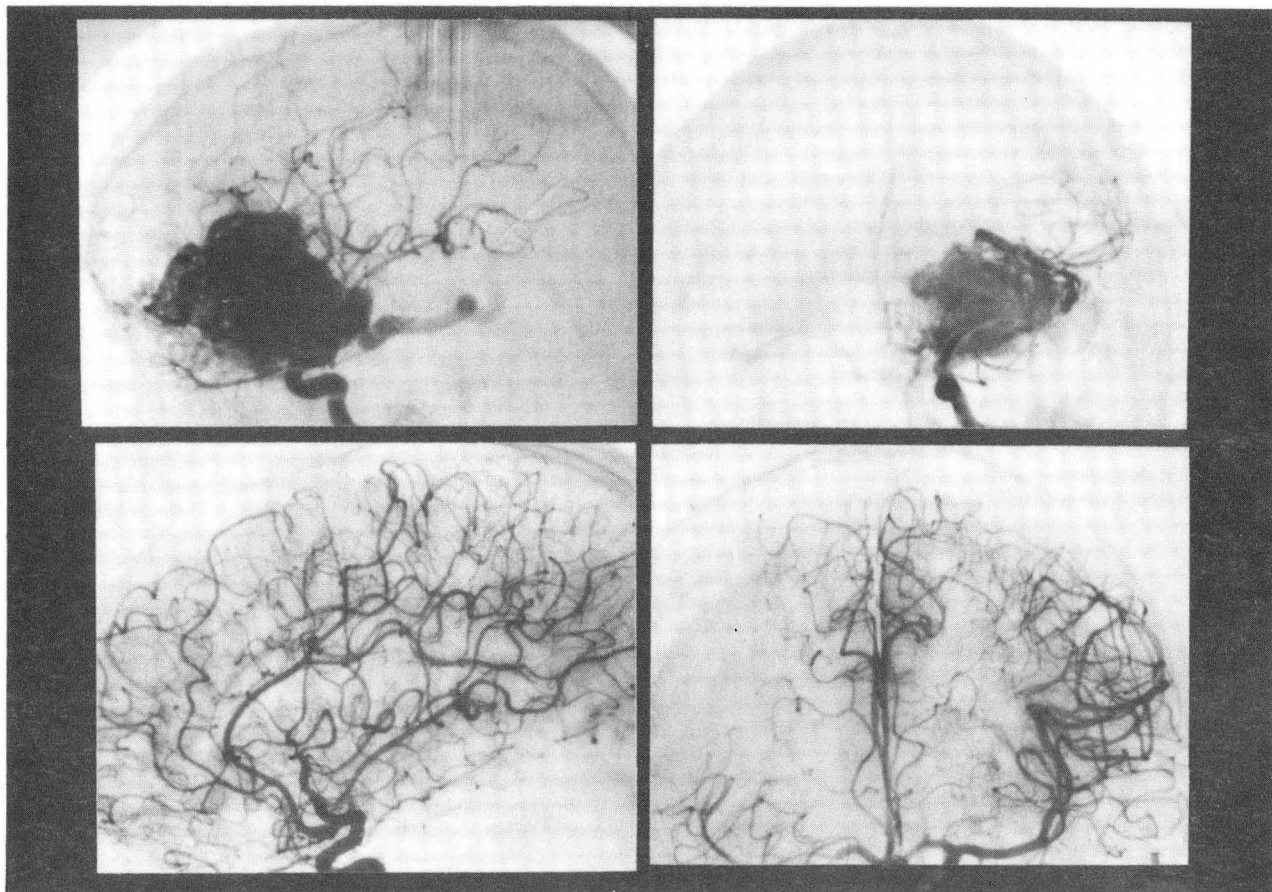
Figure 13

Figure 14

XBB 880-9976

Months after Helium-Ion Radiation
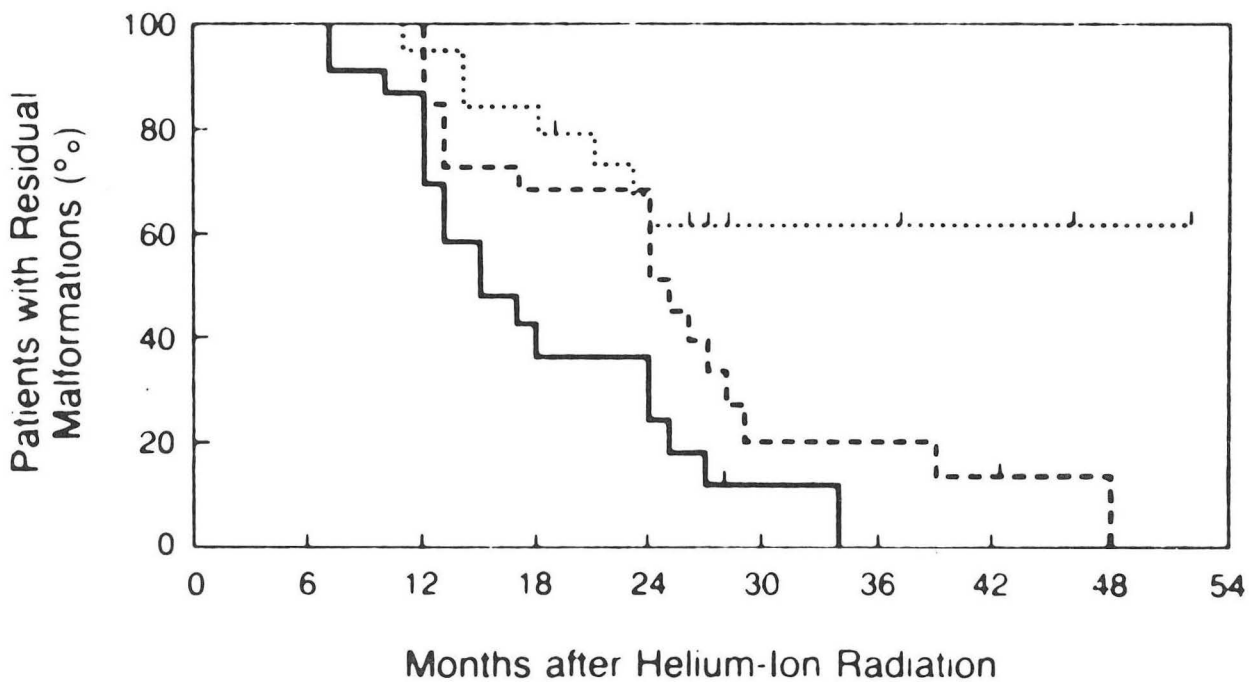
XBL 9011-3698

Figure 15
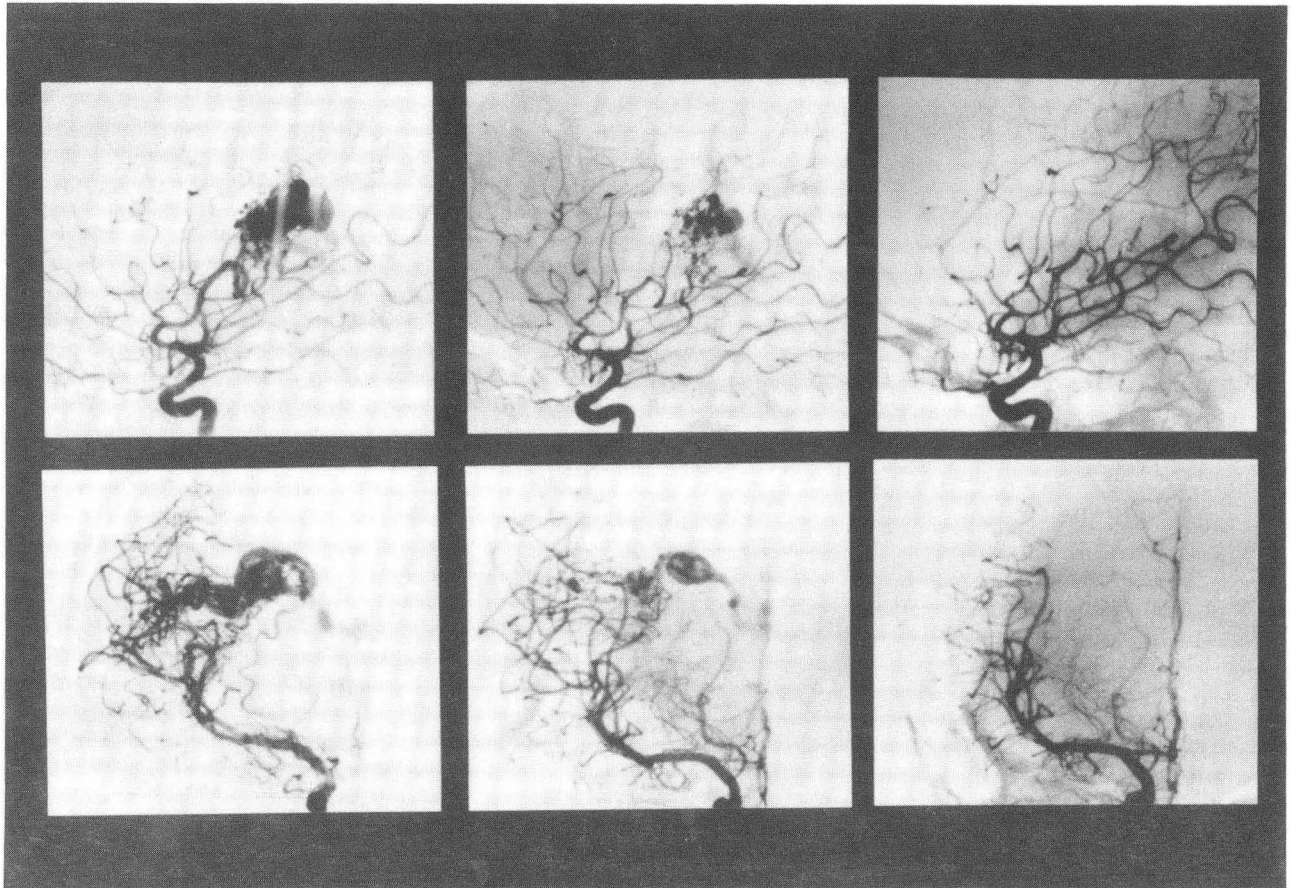
XBB 894-3556

Figure 16
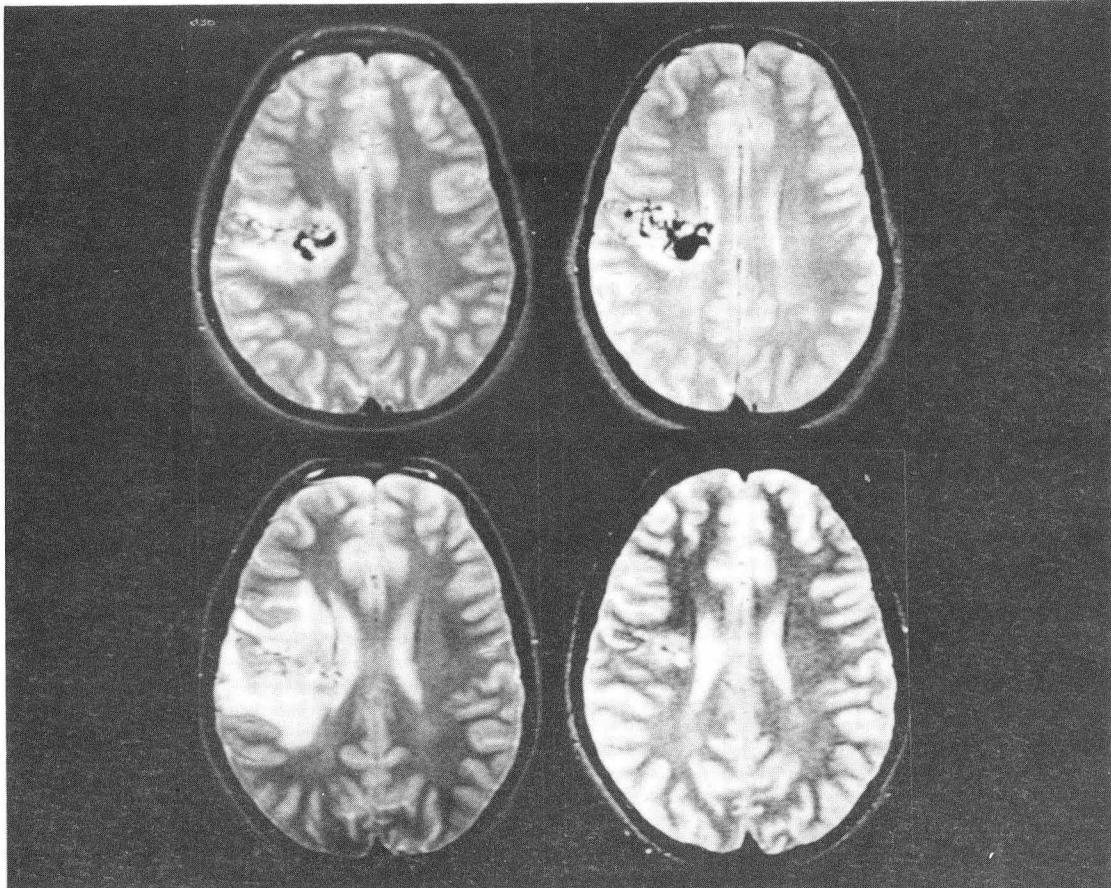
XBB 894-3557

Figure 17
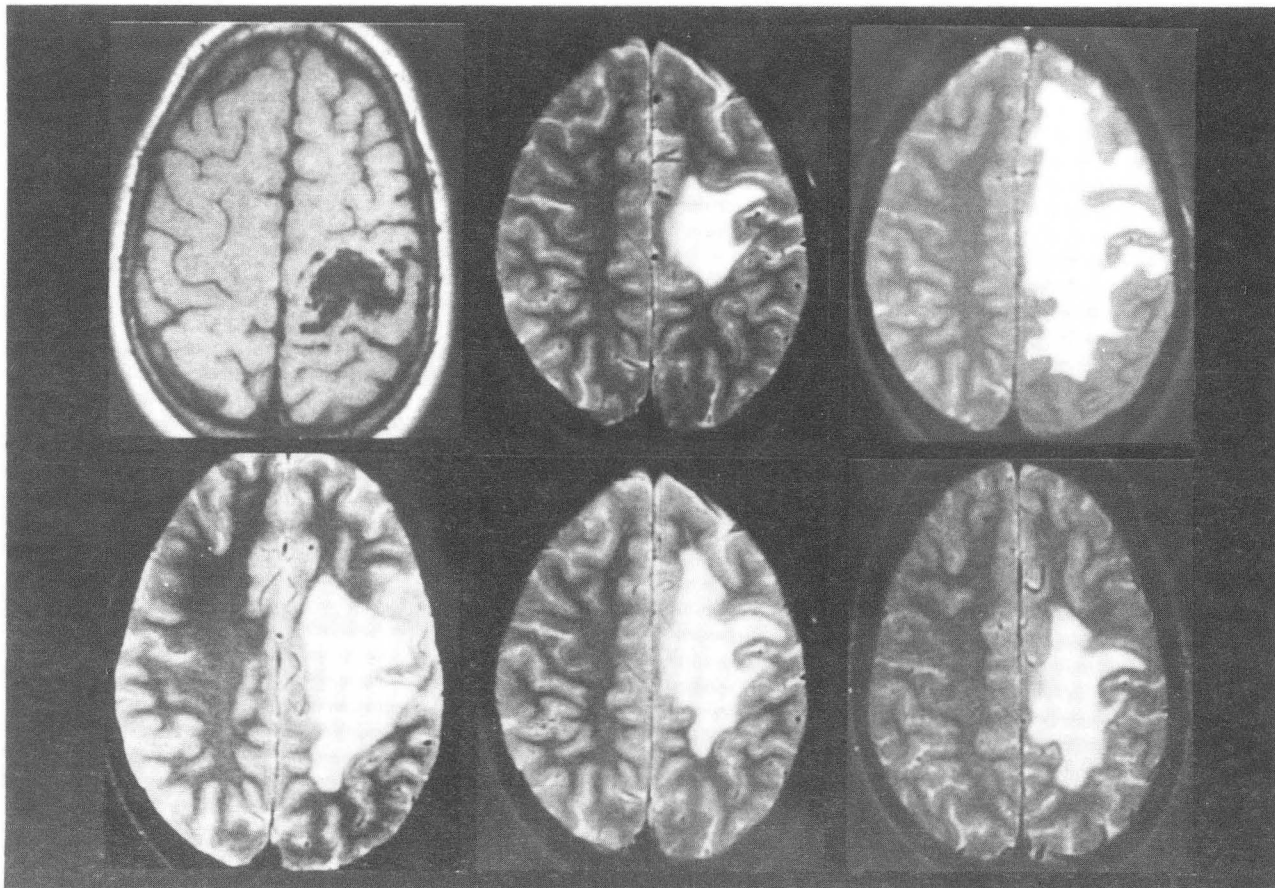
XBB 884-4125

Figure 18
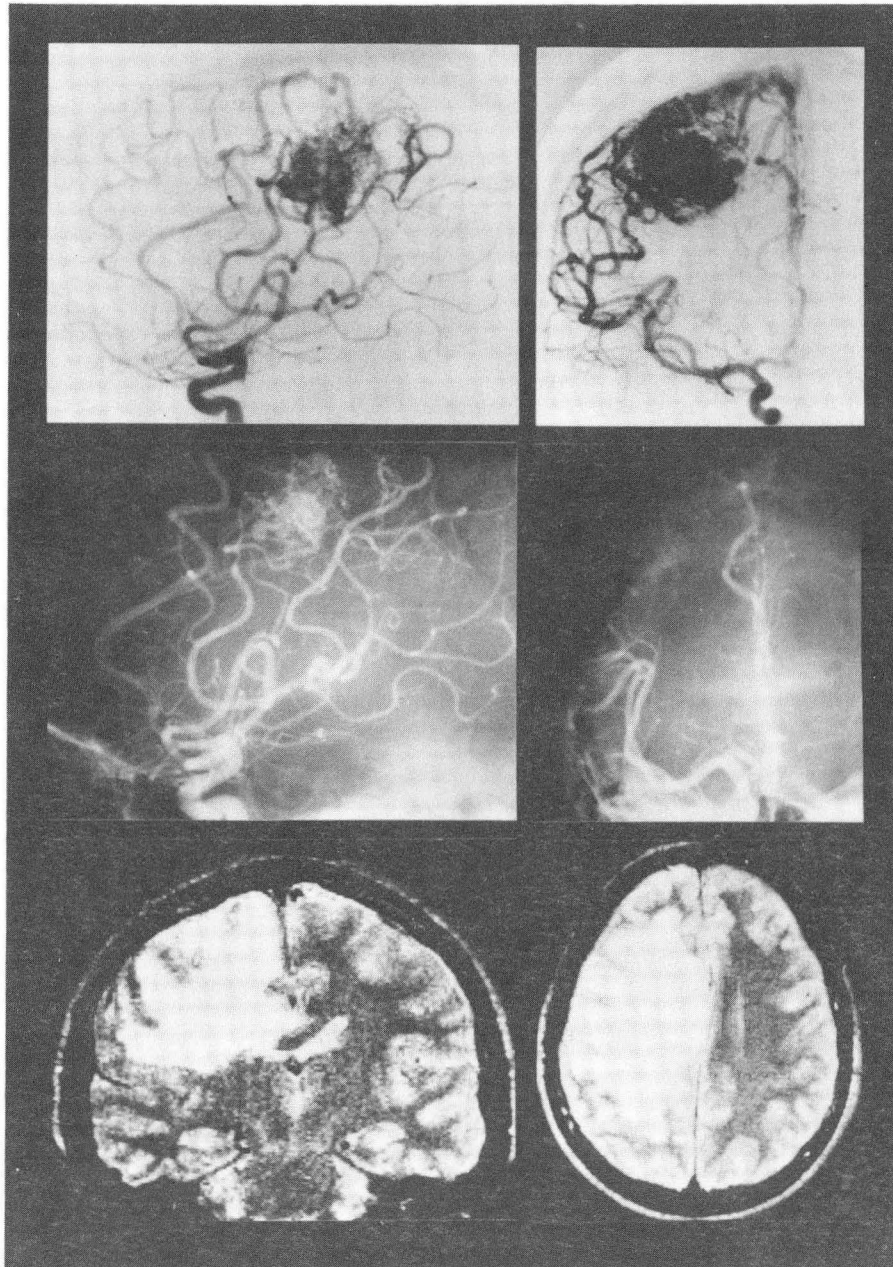
XBB 894-3549

Figure 19

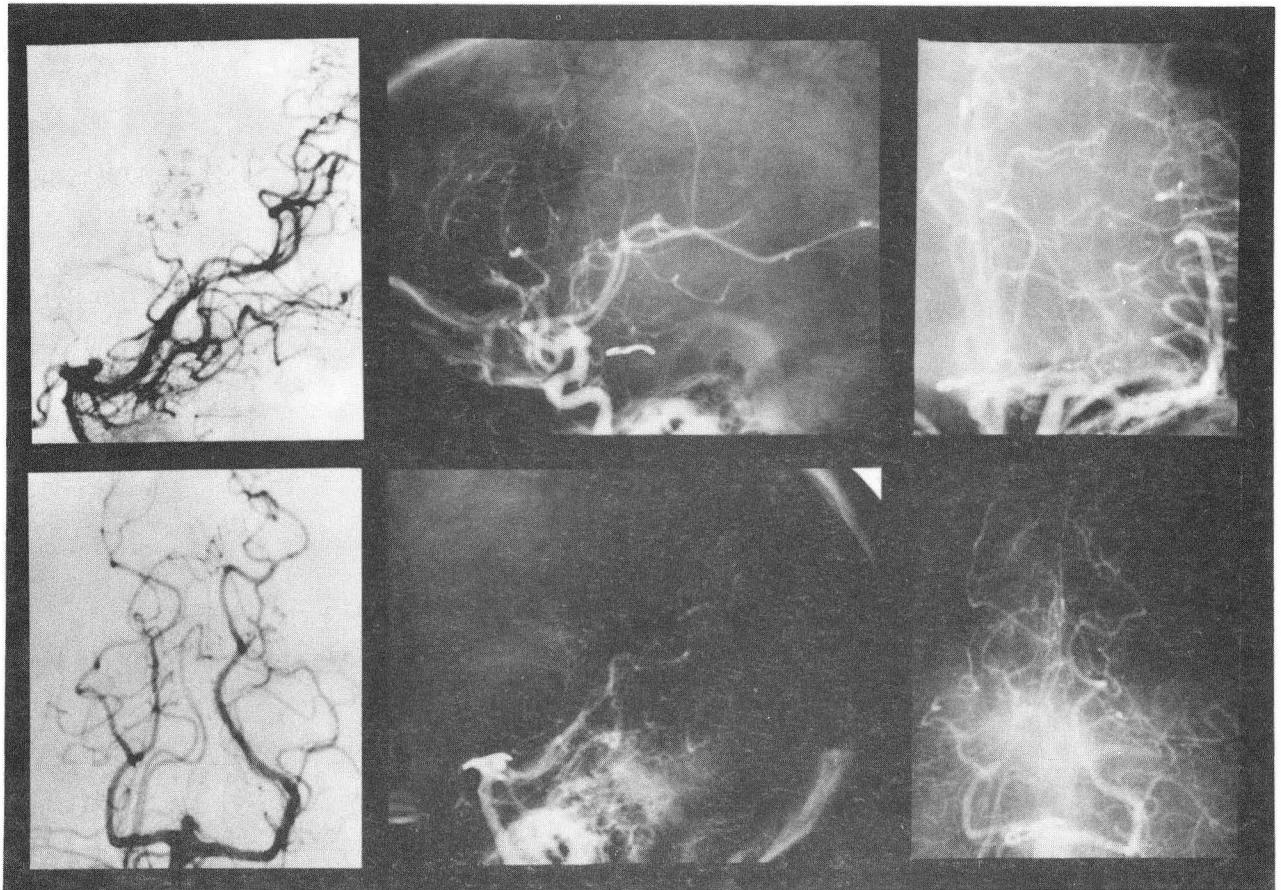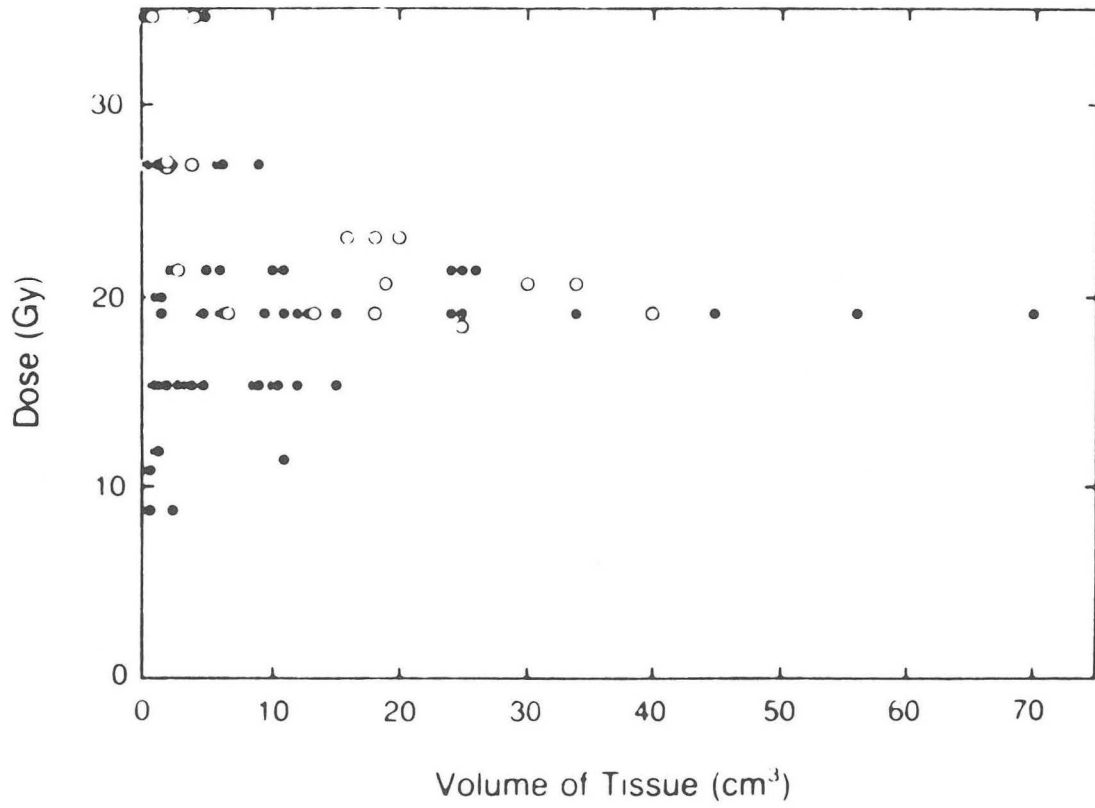# PET 600 NMR
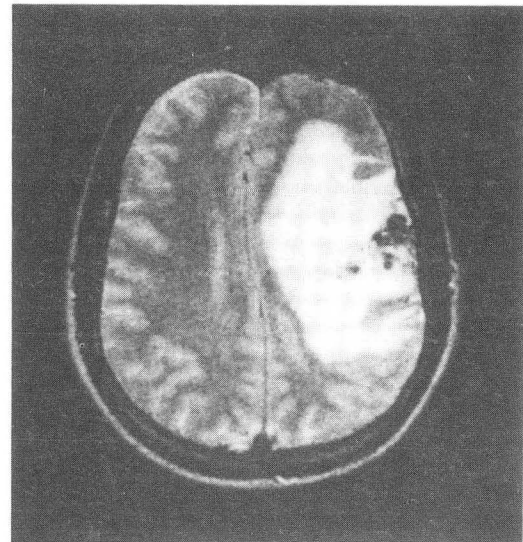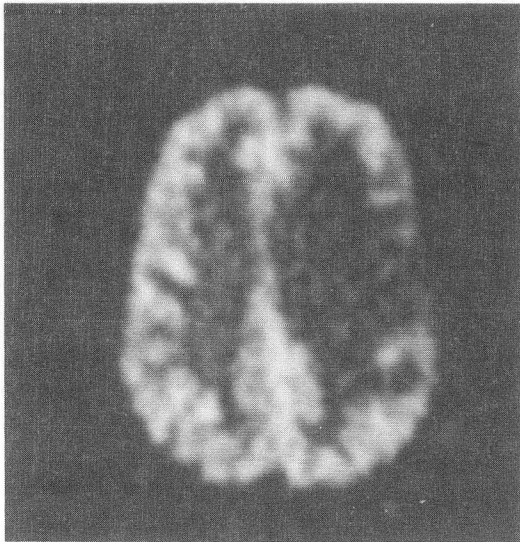
XBB 887-7044

Figure 20
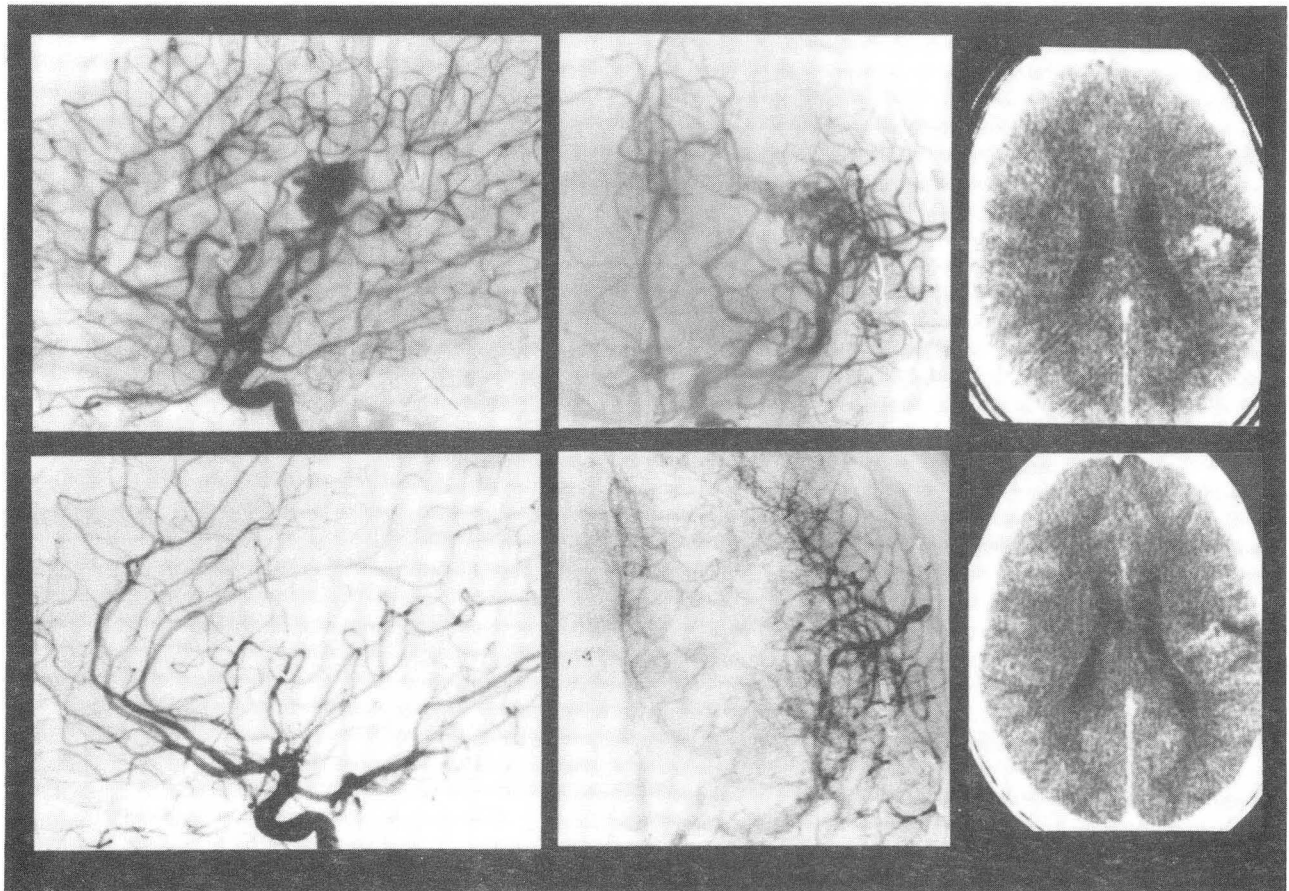
Figure 21

XBB 894-3555
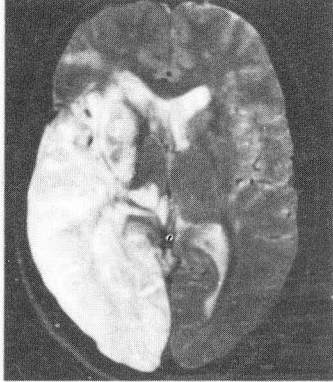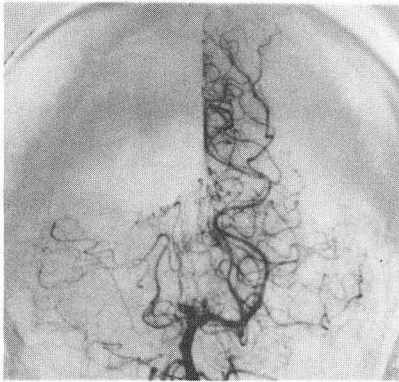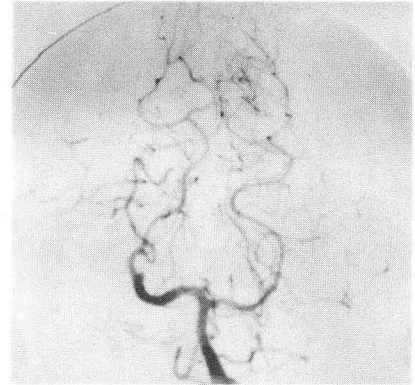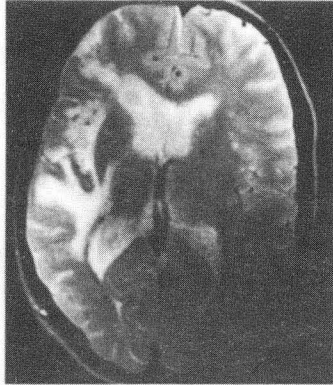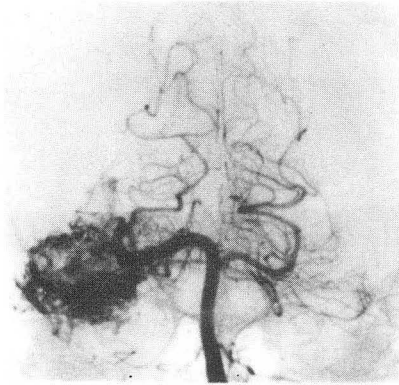
XBB 888-7620

Figure 22
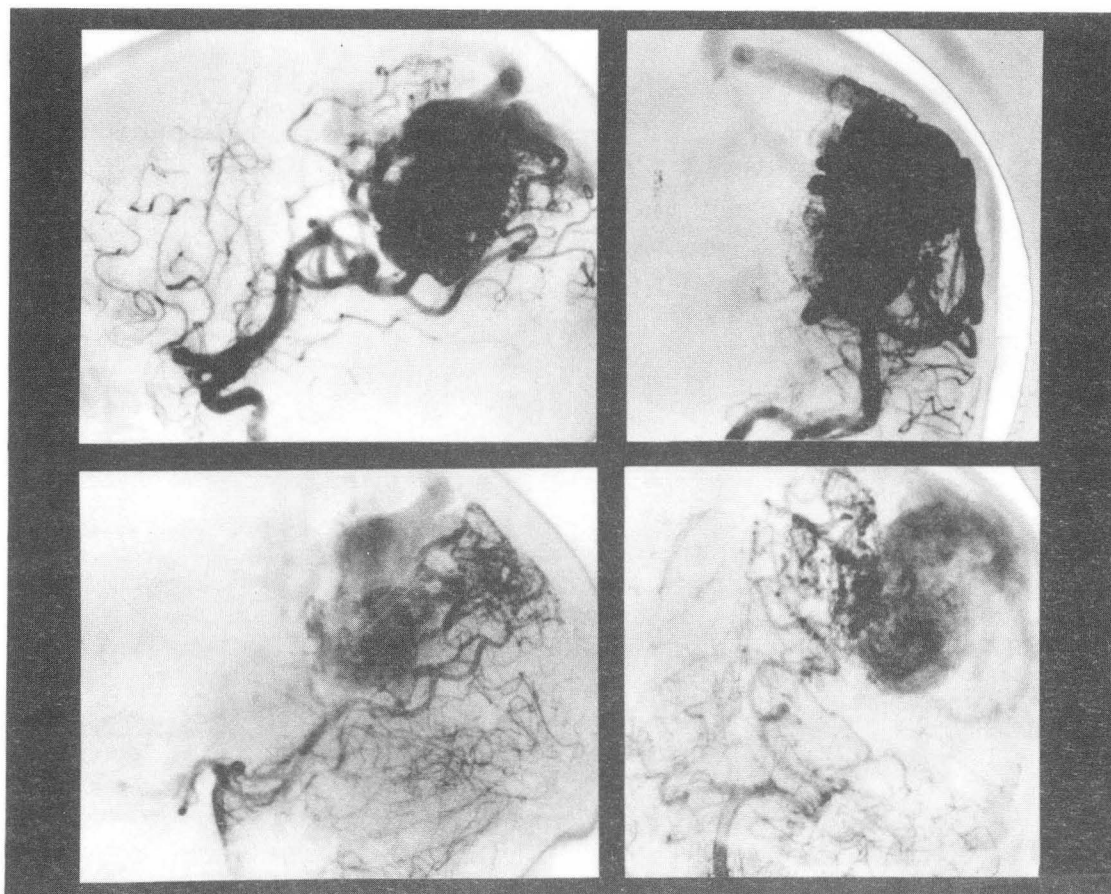
XBB 894-3550

Figure 23

XBB 894-3551

Figure 24

Figure 25

Figure 26

XBB 880-10057

	Rb-82	F-18-FDG	I-122-HIPDM
21 months			
33 months			
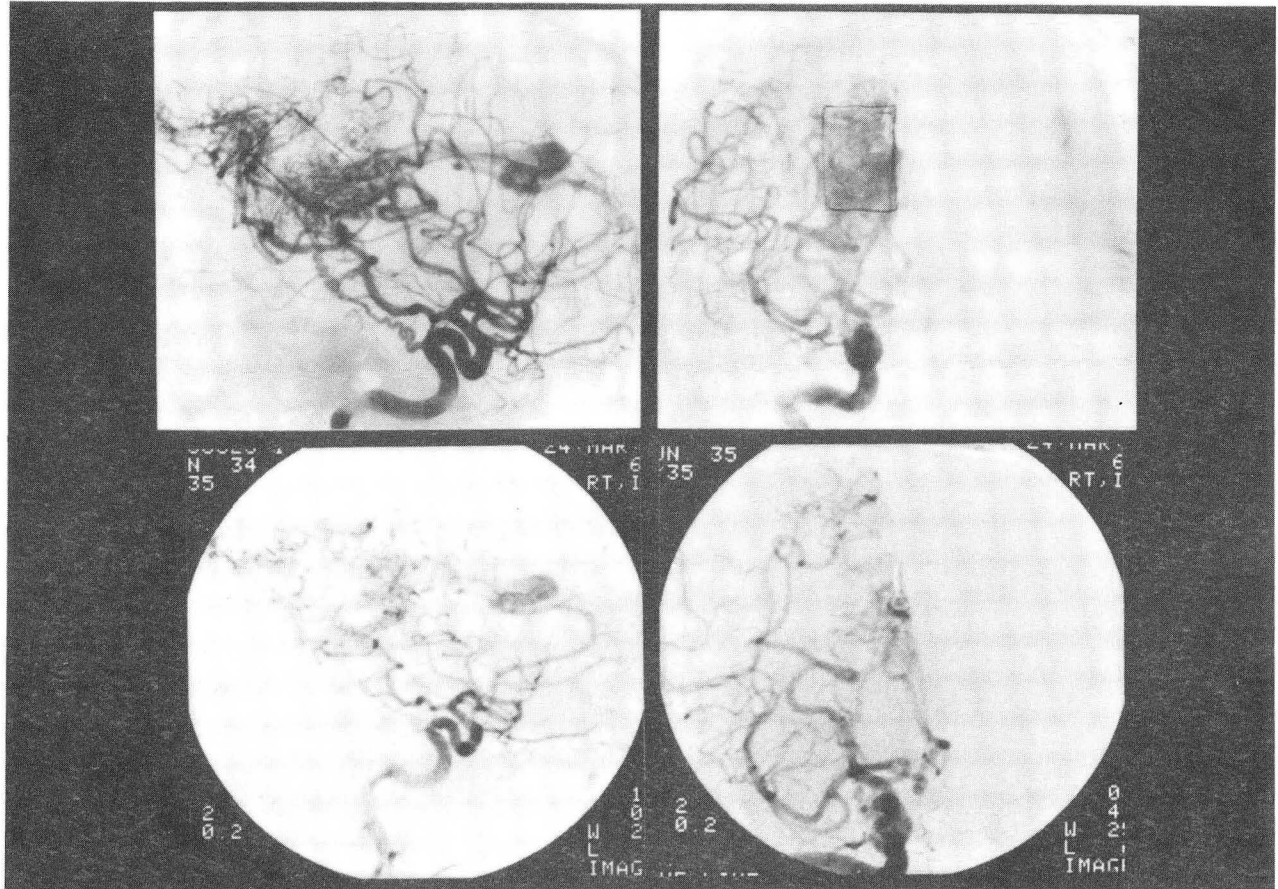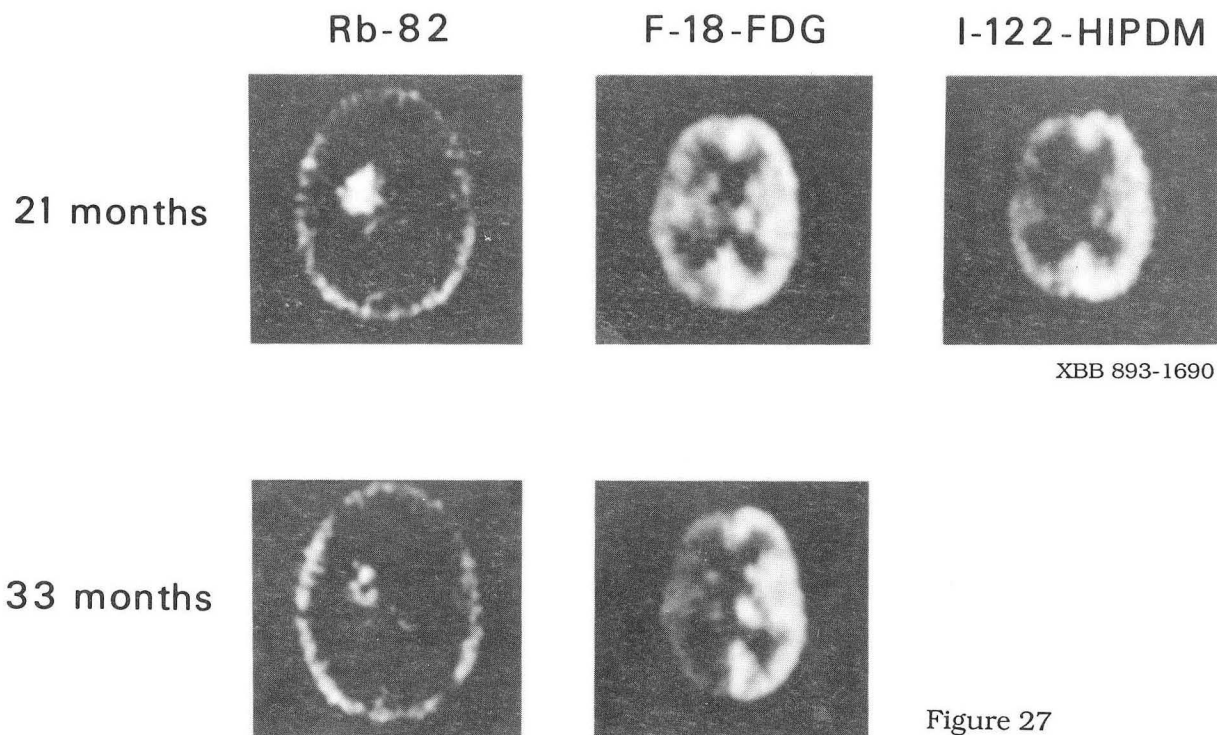
XBB 893-1690

Figure 27

XBB 852-1629

Figure 28